# In Situ Measurement of Metal-ligand Complex Dissociation Rates in Cave Dripwaters

A thesis

submitted in partial fulfilment

of the requirements for the degree

of

**Master of Science in Faculty of Science and Engineering**

at

**The University of Waikato**

by

**Xiaoli Guo**


THE UNIVERSITY OF
WAIKATO
*Te Whare Wānanga o Waikato*

2019

# Abstract

The purpose of this study was to develop a new method for determining the trace metal binding properties of natural organic matter (NOM) in cave dripwaters. The methodology is based on the diffusive gradients in the thin-films (DGT) technique, but differs from DGT by using advective gradients along hydrogel to resolve temporal trends in dissociation. For this reason, it is referred to as advective gradients in thin-films (AGT).

NOM is a ubiquitous component in natural waters. The complexation capacities of NOM ligands for metal ions in cave waters has a great impact on the transport of trace metals to, and their incorporation in, calcium carbonate cave deposits (speleothems). The relationship between the kinetics of metal-NOM complexes and the concentration of the metal-carbonate solid solution in actively forming cave precipitates, is the major focus in this study. The primary goal of this research is the determination of the mean kinetics of compositionally-unknown metal-NOM complexes in situ with the application of AGT.

The first part of this study was to calibrate the self-assembled AGT device containing a resin gel (for the binding of metal ions). A range of drip rates was tested to establish the relationship between drip rates and flow velocity within the gel with the aim of establishing a calibration function between drip discharge and flow rate within the gel. The second part of this study was to validate the method using metal-ligand complexes of known character. Synthetic solutions containing organic ligands at known concentrations were measured. The experimental data

showed acceptable reproducibility, and the modelling results agreed well with the literature.

After the laboratory-based study of the AGT method, the device was deployed in Aranui Cave, which is a natural cave located in the Waitomo District, New Zealand. Four transition metals were found in both resin gel samples and the water sample. The accumulation behaviour of the metals in the Chelex-100 resin gel demonstrated the capability of the AGT method to measure trace metals bound to unknown NOM ligands in cave dripwaters. The dynamics of the dissociation of metal-NOM complexes can be reflected by the distinct dissociation patterns of the metals.

This newly developed method can semi-qualitatively determine the dissociation rates of labile and partially labile metal-NOM complexes in natural waters. However, further optimisation of the method will be required to improve the precision and accuracy of measurements. In summary, this study provides the basic framework for further research of a new palaeoclimate proxy utilising trace meta-content in speleothems.

# Acknowledgements

My heartfelt gratitude goes to my supervisor Dr Adam Hartland, for his encouragement and guidance throughout this Masters project. I would also like to acknowledge Waitomo Caves for providing permits and access to Aranui Cave. This project was funded by a Rutherford Discovery Fellowship to Dr Adam Hartland.

I would also like to express my gratitude to the support of Annie Baker and Amanda French for their assistance with sample analysis at The University of Waikato, along with the WEG team members, including Huma Saeed, Jackson White, and Mahdiyeh Salmanzadeh, for the training on DGT preparation techniques and computer modelling software.

I must also recognize my colleagues at work. My managers have been very supportive, allowing me to pursue further education in the field of science. At various time, team members have had to deal with all of my absences, and I thank them for their understanding.

Finally, I am very grateful for having the support of my family. Many thanks for the wonderful basecamp they created for me, and for my husband's great company when I was writing this thesis.

# Table of Contents

# List of Figures

# List of Tables

# Abbreviations

| | |
|---|---|
| AGT | Advective gradients in thin-films |
| DBL | Diffusive boundary layer |
| DGT | Diffusive gradients in thin-films |
| DI | Deionis ed |
| FA | Fulvic acid |
| HA | Humic acid |
| HS | Humic substance |
| IC | Ion chromatography |
| ICP MS | Inductively coupled plasma mass spectrometry |
| IDA | Iminodiacetic acid |
| ML | Metal-ligand |
| NOM | Natural organic matters |
| NTA | Nitrilotriacetate acid |
| $pCO_2$ | Partial pressure of $CO_2$ in the cave atmosphere |
| PCP | Prior calcite precipitation |
| TEMED | N, N, N', N'-tetramethylethylenediamine |

# Chapter 1 Introduction

## 1.1 Caves and palaeoclimate

Caves are underground chambers that can take many thousands of years to form. Caves are distributed all over the world and possess many geochemical and physical properties that changes in climate. In the studies of palaeoclimate and paleoenvironment, caves are the subterranean libraries hidden in the deep recesses of the Earth. Caves typically form in karstic environments, where bedrocks made of limestone, dolomite and gypsum have dissolved over time in water. The distinctive features of caves formed by this process are the rock formations known as speleothems.

Speleothems are secondary mineral deposits in the cave. Rainwater absorbs carbon dioxide in the atmosphere and picks up more dissolved carbon dioxide from plant roots and decaying vegetable matter in the soil, along with complex organic acids (humic-like materials). This weakly acidic groundwater dissolves calcite in rocks and percolates through porous rocks into caves resulting in the production of cave formations over time. When the acidic solution enters the caves, carbon dioxide escapes. This groundwater becomes supersaturated. Hence, the dissolved calcite precipitates and forms speleothems (Richards & Dorale, 2003). The property of speleothem-forming process has been summarised by Fairchild et al. (2006) as that: the infiltrating water passes from a dissolution regime to a precipitation regime primarily because they encounter a gas phase with lower concentration of $CO_2$ ($pCO_2$) than that which they have previously equilibrated. The resultant degassing leads to supersaturation of the water for

$CaCO_3$ and a tendency for calcite precipitation. The effects will be accentuated if evaporation occurs within the cave. This process is known as prior calcite precipitation (PCP). In other words, degassing is driven by the pressure difference between $CO_2$ in the cave atmosphere and that in the dripwaters, leading to calcite precipitation.

The most familiar speleothem formations are stalactite and stalagmite formations (Figure 1). The former is the conical formation drooping from the cave ceiling, while the latter is an upward-growing mound of precipitated mineral deposits formed from water dripping onto the cave floor. Another common speleothem formation, flowstones, are less well known but also invaluable in speleothem science. They are sheets of laminated deposits like waterfalls covering floor or walls of caves.

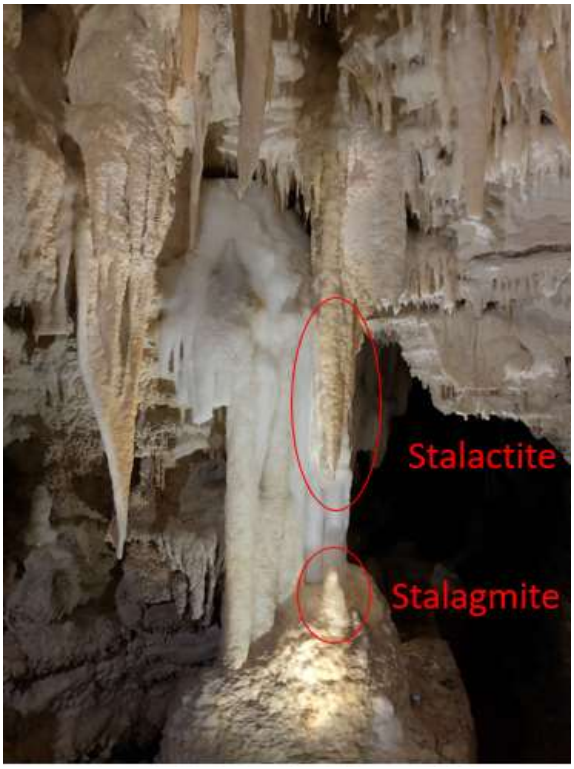


**Figure 1:** Aranui Cave features. The photograph was taken in Waitomo, NZ, March 2019.

Speleothems, particular stalagmites, have been increasingly studied as important archives preserving information about past hydrology, rainfall, temperature, soil and other past climatic and environmental conditions (Richards & Dorale, 2003).

The key advantages of speleothems as continental climate proxy recorders compared with other palaeoclimate archives, e.g. marine sediment cores, ice cores, loess sequences and tree rings for example, are that they possess multiple measurable proxies while the cost of acquisition of speleothems are relatively less expensive. For example, speleothems are widespread all over the world, but ice cores can only be drilled in high polar latitudes. The most commonly measured variable, oxygen isotope ($\delta^{18}O$), has long been utilised to reconstruct cave temperature. The results obtained from speleothem $\delta^{18}O$ have been used to challenge or refine the ice core-based glacial and interglacial periods. The reliability of another stable isotope carbon ($\delta^{13}C$) used for recovering soil and vegetation dynamics has also been extensively studied. Trace element variations have also been explored as a proxy of palaeohydrology (Borsato, Frisia, Fairchild, Somogyi, & Susini, 2007). The uranium-thorium technique has been applied to tie speleothems to time precisely and accurately. This dating technique is the most widely-used and reliable dating technique used on speleothems less than half a million years old (Richards & Dorale, 2003).

However, there are analytical constraints with the use of the above proxies. To date, interpretation of palaeoclimate from these geochemical proxies in many studies are still ambiguous due to insufficient understanding of the meaning of the proxies (Fairchild & Treble, 2009). The uranium-series dating technique depends

critically on the accuracy with which the mixed $^{229}Th/^{236}U$ spikes have been calibrated to known secular equilibrium standards. Also, systematic inter-laboratory comparisons are required to ensure the reproducibility of uranium-series dates produced by different laboratories (McDermott, 2004). The time interval represented by individual stable isotope measurements is affected by the growth rate of the speleothem chosen for analysis. Meanwhile, stalagmite growth rates depend on many factors such as temperature and the $Ca^{2+}$ concentration of the dripwaters (Genty, Baker, & Vokal, 2001). In addition, it is important to understand the factors that influence oxygen isotope ratios in the cave waters of individual drip systems, in order to interpret the oxygen isotope fluctuation correctly (Hellstrom & McCulloch, 2000).

Despite speleothems having more inherent complexities than other palaeoclimate archives, process studies and instrumental development over the past couple of decades have obtained high-resolution multi-proxy records for robust interpretation and have minimised distortion of chemical signals (Fairchild et al., 2006). Cruz et al. (2007) used multi-proxy measurements to interpret the changes in trace element ratios (Mg/Ca, Sr/Ca), reflecting local rainfall patterns and their covariations with $\delta^{18}O$ in the same speleothem. This research provided invaluable information on palaeohydrological conditions. Because trace element variations are controlled by local variables such as groundwater conditions, prior calcite precipitation and the evolution of the flow regime, which are highly influenced by rainfall changes (Scroxton et al., 2018).

Further research into the mechanism of trace elements incorporation in speleothems would be beneficial for gaining greater insight into utilising these chemical signatures for the determination of paleoclimate proxies.

## 1.2 Trace elements in speleothems as palaeoclimate proxies

Speleothem trace metal concentrations (magnesium, strontium, uranium, copper, zinc) and their ratios to calcium are increasingly used as alternatives, or to supplement $\delta^{18}O$ values, for investigating climatic events that disrupted the local hydrological cycle. The regular annual cycles of trace element variations in speleothems also have been studied for chronology reconstruction. With the advancement of analytical techniques in recent years, more and more palaeoclimatically significant results have been generated. For example, laser ablation inductively coupled plasma mass spectrometry, atomic absorption spectrometry and secondary ionisation mass spectrometer have extended our general knowledge of the capability of $CaCO_3$ minerals to incorporate trace species. The combined use of an electron microprobe and micro X-ray fluorescence spectrometer using synchrotron radiation has enabled the mapping of chemical elements within the speleothem. However, there are limitations with each technique, such as high detection limits, destructive sampling protocols, compromised precision and accuracy of the results, analysis throughput and cost of the analysis (Fairchild & Treble, 2009).

Chemical species in speleothems originate from atmospheric precipitation, bedrock, sediment, and elements recycled via soil biota (Figure 2). Calcite and

dolomite in bedrock and the overlying soil zone are the two most important sources of ions in cave waters (Fairchild et al., 2006).

It is important to understand the processes involved in the karst system controlling metal speciation to use these proxies for revealing past climate changes. However, there are too many environmental, climatic and geologic variables that may influence the chemistry of speleothem calcite, making the interpretation of trace element variations challenging (Johnson, Hu, Belshaw, & Henderson, 2006). Fairchild et al. (2000) discussed four mechanisms that may control the trace element compositions and concentrations in cave dripwaters:

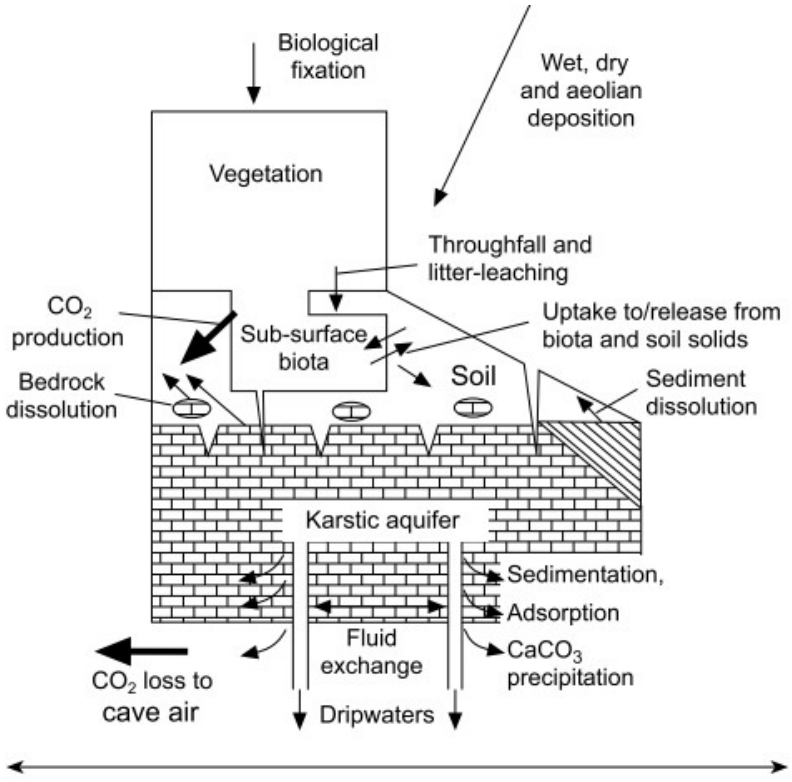


**Figure 2:** A schematic diagram indicating the various sources of elements and processes such as cave system hydrology and air circulation controlling the transport of elements into speleothem-forming dripwaters (Fairchild & Treble, 2009).

(1) Differential dissolution of calcite and dolomite affects the leachate compositions over long reaction time. Longer residence time allows for more dissolution of dolomite; therefore, increasing specific metal concentrations (i.e. magnesium) compared to calcium in speleothem-forming dripwaters.

(2) Calcite precipitation, which preferentially removes calcium ions from solution and simultaneously changes the concentrations of other metal cations based on the partition coefficient ($D_M$) of metal (M). This is expressed by the formula:

$D_M = (M/Ca)_{calcite}/(M/Ca)_{solution}$.

If $D_M << 1$, enhanced $CO_2$ degassing in drier condition would increase the ratio of metal to calcium, which can be seen from annual cycles of magnesium (Mg), strontium (Sr), barium (Ba) in speleothems.

(3) Incongruent dolomite dissolution where calcium is preferentially released from dolomite rather than calcite. The resulting trace element ratio increase is related to prior calcite precipitation as described in mechanism 2. However, this mechanism was less significant in most cases.

(4) Selective leaching of trace elements (magnesium and strontium) with respect to calcium compared with their ratios in the source material.

A study of a modern speleothem from Moondyne Cave (Australia) demonstrated the potential of speleothem magnesium as a proxy recording effective previous rainfall (Treble, Shelley, & Chappell, 2003). The enrichment of magnesium in dripwaters may be attributed to either the more trace element-rich slow-flow aquifer compartment (mechanism 1), or prior calcite precipitation (mechanism 2),

or the combination of both as they are consistent with the influences of dry conditions in caves.

Up to date, knowledge of trace elements in speleothems as climate proxies has been limited to those metals exhibit simple partitioning (magnesium, barium and strontium). However, the partition coefficient is not universal in explaining trace metal partitioning in speleothems. When there are metals which exhibit strong binding affinities to organic ligands present in the drip waters, the available metal (free metal ions and metal complexes) is much lower than the total metal in solution. For example, transition metals, particularly nickel, copper and zinc have strong binding affinities for naturally existing organic matter in waters (Warnken, Davison, Zhang, Galceran, & Puy, 2007).

As trace metal variations in speleothems have climatic significance, information on the complexation characteristics of these metals with organic matter, as well as the fraction of trace metal available for partitioning into speleothem could provide additional invaluable knowledge for palaeoclimate studies.

## 1.3 Organic matter in natural waters

Natural organic matter or NOM refers to all the organic materials in natural systems produced from the decay of plant material, other than living organisms and synthetic compounds. Therefore, NOM covers a wide range of heterogeneous polymeric substances, including humic substances (HS). In trace metal binding studies, only HS are hydrologically significant as they represent the majority of NOM in natural waters and their sediments. Aquatic HS are often divided into two

fractions as humic acids (HA) and fulvic acids (FA), based on the degree of complexation, molecular weight, solubility, and functional group distribution. FA are soluble in both acidic and alkaline conditions and have low molar masses (~1000 Da). In contrast, HA are soluble in alkaline conditions and their molar masses are higher.

In freshwaters, FA account for 40-80 % of NOM, whereas HA is mostly present in soils and sediments as part of the solid phase (Tipping, 2002). Variable sources of NOM result in vast variations of molecular compositions which impede the characterisation of NOM. For freshwaters, the range of binding sites HS possess leads to a distribution of binding constants (Warnken et al., 2007). Therefore, the well-characterised reference materials Suwannee River fulvic acid (SRFA) and Suwannee River humic acid (SRHA) are particularly useful for experiments investigating interactions between trace metals and dissolved NOM in natural waters.

It is widely accepted that NOM acts as a dominant complexing agent (termed as ligand) and that NOM plays a vital role in the mobilisation and transport of trace metals (McKnight, Hornberger, Bencala, & Boyer, 2002). For example, NOM are found to bind $CaCO_3$ in dripwaters and then co-precipitate in speleothems. This finding was supported by the fluorescent variations in speleothems as a result of seasonal fluctuation of NOM concentrations in dripwaters (van Beynen, Schwarcz, Ford, & Timmins, 2002).

In studies of metal-NOM complexes, stoichiometric methods for the determination of the poorly characterised, heterogeneous HS are difficult. Unambiguous reaction

schemes of metal-ligand (ML) complexes cannot be easily made to understand the properties of these compounds. It is also difficult to provide a detailed description of all the species present in natural waters (Sigg et al., 2006). Recent advancements in this area were made by Warnken, Davison, and Zhang (2008), who developed the theoretical basis of using diffusive gradients in thin-films technique. Using this method, they were able to derive information on the distribution of metal species in freshwaters, as well as the dissociation rates of these complexes.

To date, it is generally assumed that only the portion of trace metals that present as free metal ions will precipitate into calcite. It was previously shown that the formation of metal-organic ligand complexes prevented the absorption of metal cations by calcite (Lee, Elzinga, & Reeder, 2005). In other words, free metal concentrations are at low levels because NOM controls the forms of most metals present in natural waters. Whereas, Hartland, Fairchild, Lead, Zhang, and Baalousha (2011) argued the fractional partitioning of metals between dripwaters and speleothems was not restricted to free ions but also metal species with low stability. Dissolved metal species in natural waters were classified as “labile” and “inert” according to their NOM binding affinities. To be more specific, labile metal species consisted of free metal ions, and those ML complexes that dissociate-rapidly in the presence of calcite surfaces, while inert complexes dissociated much more slowly.

In this study, we are using the labilities of metal-NOM complexes to describe the incorporation of previously complexed metals in speleothems. Inert metal species

have zero partitioning but may co-precipitate on the mineral surface. In contrast, labile ML complexes dissociate in the thin water film at the stalagmite surface. The metal ions compete for binding sites at the calcite surface. Therefore, those metals with high affinity for calcite surface sites (relative to NOM) are expected to be stripped from NOM (at a defined rate) then adsorbed onto calcite.

## 1.4 Challenge of characterising the process at the speleothem-forming surface

Little is known about the metal transformation process at the speleothem forming surface. One of the difficulties for this type of analysis comes from making accurate measurements of chemical speciation directly on natural waters. To measure the metal species directly, the methods must be both very sensitive for low concentrations and specific for the distinction between chemical species (Unsworth et al., 2006). The measurements can be performed either in situ or in-laboratory. However, analysing samples in the laboratories has a higher risk of introducing contamination. Moreover, metal speciation in the samples may change during transport, storage, and sample pre-treatment procedures due to the changes of temperature, pH and bioactivity, for example. Low concentrations of trace elements in natural waters also contribute to the challenge of measurements. Stringent protocols for extraction and ultra-clean tools and consumables are required to avoid metal contaminations.

Metal speciation modelling from measurements of total metal concentrations is a common approach to determining the metal species associated with inorganic

ligands, as they are relatively simple and well understood. However, it is complicated to use these models to predict metal-NOM complexes, because of the unknown nature and concentrations of NOM in natural systems. Although the total organic carbon (TOC) content of the water can be measured using well-proven analytical techniques. Part of this TOC is often assumed to behave like HS, while part of it is likely to be inert for metal ion binding. In addition, as the major ligands in natural waters, HS have a range of binding sites with a distribution of binding constants, giving diverse dissociation rate constants. This also makes it difficult to characterise naturally occurring metal-organic ligand complexes and to appropriately interpret the data (Warnken et al., 2007).

Overall, in situ measurements are the most desirable to obtain the true value of the mean effective dissociation rate. The ratio of metal to ligand is crucial for determining the rate. Because of the possible modelling error and uncertainties, these models must be tested by comparing predicted values with experimentally determined results (Kalis, Weng, Dousma, Temminghoff, & Van Riemsdijk, 2006).

## 1.5 Study Objectives

The aim of this research project is to develop a new method to characterise the labilities and dissociation rates of metal-NOM complexes in cave dripwaters. The measurements will assist in understanding the process of trace metal incorporation into speleothems and the associated trace metal signals. Once validated, this new method will contribute to studies aimed at developing novel quantitative proxies of past climate from speleothems.

### 1.5.1 Objective 1

The so-called AGT channel probe is a novel sampling device based on the design of diffusive gradients in thin-films (DGT) sampler. In order to understand the movement of solution within the gel fixed in the probe, in-laboratory calibration will be performed. The drip rate and the distance the tracer travels will be used to calculate the time available for ML complex to dissociate.

### 1.5.2 Objective 2

With the knowledge gained from how solutions travel within the gel in the AGT channel probe, the probe will be exposed to a set of well-mixed nickel test solutions to model metal transfer under laboratory conditions. This section of study will compare the characteristics of the known metal-organic ligand complexes determined by our AGT approach with comparable data from the literature. This approach will determine whether this method is suitable for measuring unknown ML complexes in natural waters.

### 1.5.3 Objective 3

A field experiment will be carried out to examine the practical application of the channel probe to measure ML complexes in an underground cave environment.

# Chapter 2 Methods and Materials

The project was divided into four components: channel probe preparation, determination of flow movement within the resin gel using an inorganic tracer, metal accumulation study using synthetic metal-organic ligand solutions and deployment of the calibrated channel probe in a natural cave.

Clean laboratory facilities and stringent protocols are required to avoid or limit contamination issues. All laboratory work was carried out in the Chemistry Research Lab D3.12 at The University of Waikato. The glass plates (Figure 3), gel cutter (Figure 4) and acrylic channel probe (Figure 5) were manufactured at the Science & Engineering Workshop of The University of Waikato. The binding gel was fabricated and tailored in a laminar flow cabinet with filtered air. All chemicals are of analytical reagent grade or better unless specified. Deionised (DI) water was used for all preparations, including the cleaning of glassware and containers. Prior to the experiments, plastic forceps, spacer, glass plates, channel probe parts and filter paper strip were double acid-washed. All utensils were soaked in 10 % (v/v) HCl for at least 30 min, followed by soaking in 10 % (v/v) $HNO_3$ for another 30 min, then rinsed thoroughly with DI water and dried under the air stream in the lamina flow hood.

## 2.1 Reagent

All reagents are of analytical grade unless specified.

(1) Deionised water (DI water), resistivity at 25 °C > 18.2 MΩ·cm

(2) DGT gel cross-linker, 2 % aqueous solution, DGT Research Ltd. Lancaster, UK

(3) Acrylamide solution, 40 % w/v, CAS#1610140, Bio-Rad Laboratories, Inc.

(4) Ammonium persulphate, CAS# 7727-54-0, Merck

10 % w/v ammonium persulphate solution: weigh 0.100 g of ammonium persulphate and add 1 mL of DI water. Prepared before use.

(5) N,N,N',N'-tetramethylethylenediamine (TEMED), CAS# 110-18-9, Bio-Rad Laboratories, Inc.

(6) Chelex resin 100, sodium form, 200-400 mesh, Bio-Rad Laboratories, Inc.

Weigh about 5 g of Chelex 100 resin into a clean falcon tube. Add 30 mL of DI water and soak for 1 h before use. Decant the excess water from Chelex to leave a stiff slurry.

(7) NaCl, CAS# 7647-14-5, 58.44 g/mol, Merck

0.05 M NaCl solution: weigh 1.461 g of NaCl. Dissolve and dilute with 500 mL of DI water.

(8) $Na_2HPO_4$, CAS# 7558-79-4, 141.96 g/mol, BDH Chemicals

***Buffer 1***, 0.01 M $Na_2HPO_4$ solution: weigh 1.420 g of $Na_2HPO_4$ and transfer into a 1 L volumetric flask. Make to volume with DI water. Prepared daily.

(9) $NaH_2PO_4 \cdot 2H_2O$, CAS#13472-35-0, 156.01 g/mol, BDH Chemicals

***Buffer 2***, 0.01 M $NaH_2PO_4$ solution: weigh 0.390 g of $NaH_2PO_4$ and transfer into a 250 mL volumetric flask. Make to volume with DI water. Prepared daily.

(10) $NaNO_3$, CAS#7631-99-4, 85 g/mol, Merck

***Resin gel storage solution***, 0.01 M $NaNO_3$ solution: weigh 0.850 g of $NaNO_3$ and transfer into a 1 L volumetric flask and make to volume with DI water.

(11) pH 8.0 phosphate buffer solution: mix 53 mL of buffer 1 and 947 mL of buffer 2. Add 0.85 g $NaNO_3$ to adjust ionic strength.

(12) Nickel standard solution, 1000 mg/L, Sigma Aldrich, atomic absorption spectroscopy grade.

(13) Nitrilotriacetic acid (NTA), CAS# 139-13-9, 191.14 g/mol, BDH Chemicals.

(14) $HNO_3$ 70 %, Fisher Chemicals, trace element analysis grade.

***Extractant***, 1 M $HNO_3$ solution: dilute 6.4 mL of concentrated $HNO_3$ with 93.6 mL of DI water.

## 2.2 Preparation of channel probe

The preparation procedure was adapted from the manual for DGT sampler fabrication provided by Lehto (2016).

### 2.2.1 Gel stock solution

Gel stock solution consists of 15 % (v/v) acrylamide solution and 0.3 % agarose cross-linker. Weigh 7.5 g of 2 % DGT gel cross-linker into a clean 50 mL falcon tube. Using an adjustable pipette, add 23.8 mL of DI water and 18.7 mL of 40 % acrylamide solution. Mix thoroughly.

The gel stock solution can be stored at 4 °C in the dark for up to 3 months.

### 2.2.2 Resin gel casting

To make a Chelex resin gel sheet, weigh 4 g of moist Chelex 100 resin into a 60 mL flat bottom tube. Using adjustable pipettes, add 10 mL of gel stock solution, 120 µL of 10 % ammonium persulphate solution (as initiator) and 28 µL of TEMED catalyst. Mix well. Air bubbles in the gel should be avoided. Thus, stirring is preferred to shaking as this will reduce the potential for foam to form.

Care should be taken not to wait too long as the TEMED will initiate polymerisation of the gel solution. The solution must be immediately cast between the glass plates assembly (Figure 3). Lay the glass plates horizontally in a pre-heated 43 ± 2 °C oven for 45 min to allow the polymerisation to occur. The resin beads would settle on one side of the gel by gravity during casting.

a

b

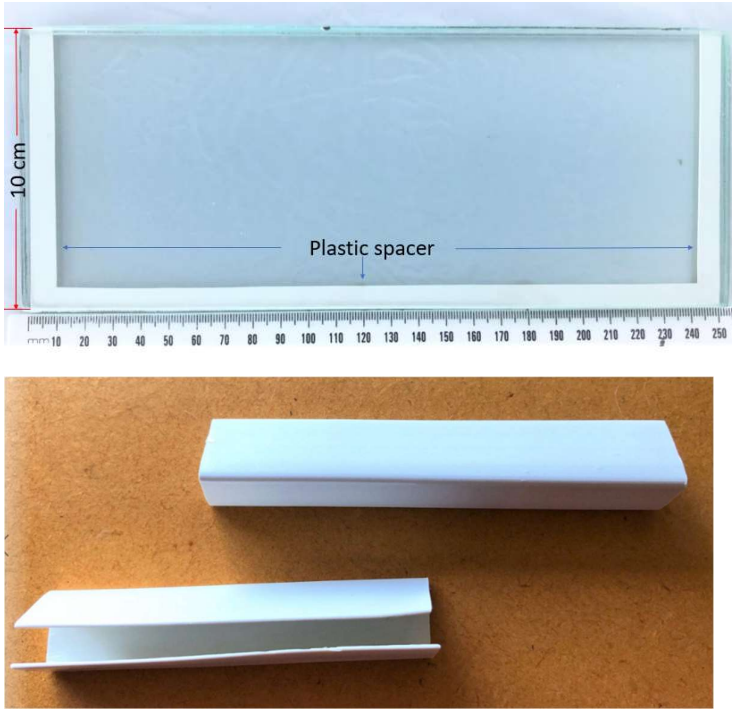


**Figure 3:** (a) The U-shape plastic spacer (thickness 0.5 mm) sandwiched between glass plates (dimension 10 x 25 cm). (b) The assembly was secured by plastic clips before the resin gel mixture was infused.

Once the resin gel has polymerised, the glass plate assembly was taken out from the oven and cooled to room temperature. A small amount of DI water was dropped into the gap of the assembly before prying the glass plates apart. The set gel sheet was carefully removed from the plates using clean forceps and then hydrated in DI water for 48 h with at least three changes of water. This allows unreacted amides to diffuse through the gel and be removed. Note that the pH of the rinse water should be lower than 7.0. Hydration also ensures the dimensional stability of gel sheets before the cutting step.

As it is very easy to contaminate the gel, caution must be exercised throughout the whole experiment to prevent exposure of the gel to non-targeted sources of metals, as Chelex 100 binding gel readily binds any trace metals it contacts. For long term storage, the gel sheet should be stored in 0.01 M $NaNO_3$ solution at room temperature. Under these conditions, the gel sheet has a shelf life of twelve months (William Davison, 2016).

### 2.2.3 Binding gel strip cutting

**Figure 4:** The bespoke gel cutter with replaceable Teflon-coated blades laying on the acrylic chopping board.

Remove the hydrated gel sheet from the container and place it on an acid-cleaned chopping board without stretching it. Use the forceps to spread out the corners gradually.

The gel sheet was cut into 1 × 30 cm strips by pressing the gel cutter (Figure 4) firmly onto the gel to ensure a clean cut. An additional Teflon-coated blade was also used to aid in cutting. Only the portion of gel with a consistent distribution of Chelex beads was used. All gel strips were stored in 50 mL falcon tubes with 0.01 M $NaNO_3$ separately to minimise the risk of contamination. The gel strip was reused in flow rate experiments, while in metal accumulation experiments and field experiment the gel strips were for single use and divided into 1 cm sections immediately after being employed.

### 2.2.4 Filter membrane preparation

0.45 µm filter paper strips with dimensions of 1.3 × 30 cm were cut from a sheet of polyethersulfone (PES) membrane filters supplied by Sterlitech Corporation.

### 2.2.5 Channel probe assembly

The channel probe (Figure 5) was self-assembled. The binding gel strip was placed on the backing plate while the rougher side (the side with resin beads) was facing upwards. However, it is difficult to see the transparent beads once the gel is removed from the solution. This step was performed by using a glass rod to lift the gel strip in solution as folding in half. The rough side should be bending inward.

Place the strip carefully in the channel and use the forceps to unfold. Trim any excess gel.

The wetted filter membrane was overlaid on the binding gel. This was then covered with the upper/retaining plate and the assembly was secured in place with clips along the flanks of the probe. Note that nylon bolts were supposed to be used instead of clips, but they were not available for use in this project. Clips were used in the premise of guaranteeing “metal contamination free”, and no leakage was observed in the experiments. The filter membrane should be hydrated before assembling to prevent entrapment of air bubbles. The device was deployed immediately once assembled as the gel was not allowed to dry.

The assembled channel probe was positioned at 15° inclination to allow the deployment solution dripping from the head of the probe to pass through the “gutter” (Figure 5c). A peristaltic pump regulated the flow rate of drip source stored in the reservoir. The drip point was positioned hanging 2-3 cm above the beginning of the channel probe.

a

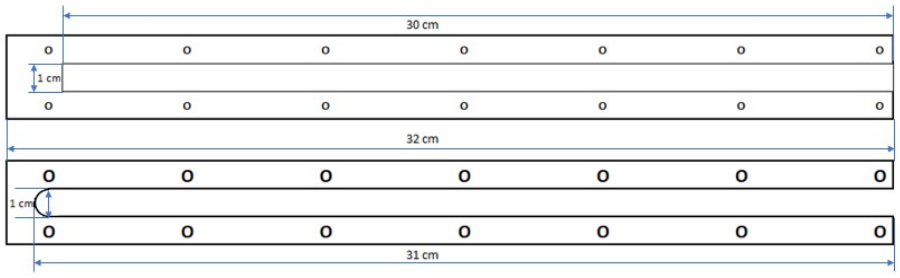


b

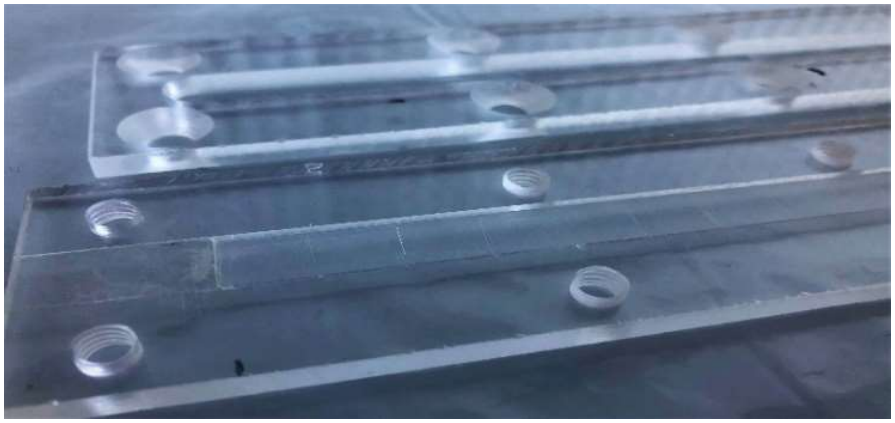

c

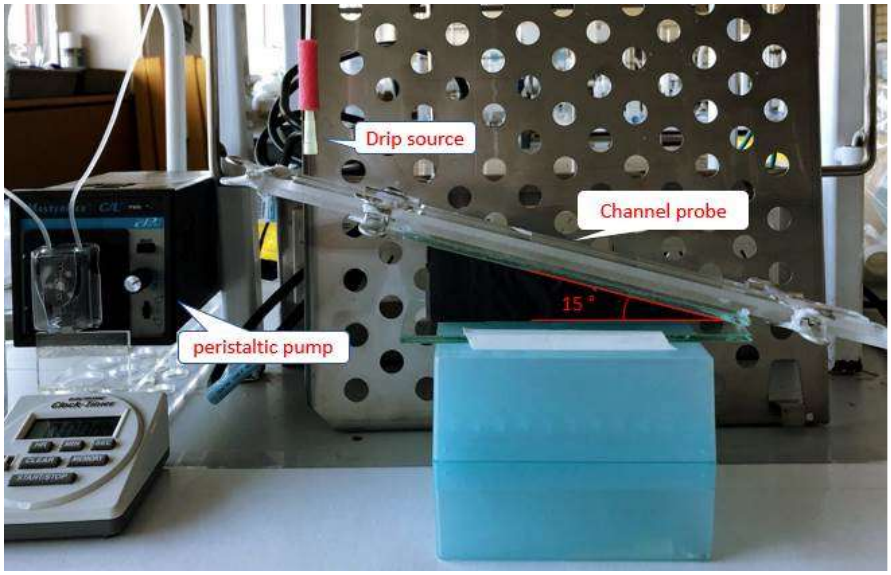


**Figure 5:** (a) Channel probe design and dimensions (top: backing plate; bottom: retaining plate). (b) This photograph shows the retaining acrylic plate with clearance holes in the back, and the backing acrylic plate with a 1 cm (W) x 30 cm (L) x 1 mm (D) gutter and female thread in the front. (c) The assembled channel probe is sitting on the holder which has a 15° inclination angle. Flow rates were calibrated before and after each experiment to ensure the consistency of solution delivery.

## 2.3 Analytical methods

For this section of work, target analytes in samples were quantitatively determined using two laboratory instruments, ion chromatography (IC) and inductively coupled plasma mass spectrometry (ICP-MS).

Analysis of chloride ions ($Cl^-$) as an inorganic tracer in the flow rate experiment was carried out on a Dionex ICS-2000 system equipped with Chromeleon 7 software at The University of Waikato. The ion chromatographs were calibrated using a set of external calibration standards, which was prepared from Dionex Seven Anion Standard II (product# 057590) to ensure accuracy. The detection limit of chloride in water was 0.5 mg/L.

Each IC sequence consisted of 2-3 pre-run positions containing either DI water or tap water to monitor the performance of the instrument. At the end of each sequence, one sample blank (DI water) was analysed to check carry-over of analyte in the column.

Regarding the metal accumulation experiments, trace element concentrations in Chelex resin were determined using an Agilent 8500 quadrupole ICP-MS, operated by skilled staff at The University of Waikato.

All ICP-MS runs included a certified reference material and internal standards to ensure the accuracy of results and minimise the drift. The instrument was set to recalibrate every 50 samples. Drift was corrected in off-line processing before raw data files were generated.

Isotopes measured in cave water samples were $^{11}B$, $^{23}Na$, $^{24}Mg$, $^{27}Al$, $^{31}P$, $^{34}S$, $^{39}K$, $^{44}Ca$, $^{51}V$, $^{52}Cr$, $^{55}Mn$, $^{56}Fe$, $^{59}Co$, $^{60}Ni$, $^{65}Cu$,$^{66}Zn$,$^{68}Zn$,$^{88}Sr$,$^{89}Y$, $^{95}Mo$, $^{107}Ag$, $^{111}Cd$, $^{137}Ba$,$^{139}La$, $^{140}Ce$, $^{153}Eu$, $^{207}Pb$, $^{238}U$.

Quantitation limits were 0.3 µg/L for Cr, 1 µg/L for Cu, 0.4 µg/L for Ni, 0.2 µg/L for Y, 2 µg/L for Zn, 70 µg/L for Na and 100 µg/L for Ca, respectively.

All pH and electric conductivity readings were taken on a benchtop Eutech pH 700 meter and a Jenway 4520 conductivity meter, respectively.

# Chapter 3 Results and Discussion

## 3.1 Background

### 3.1.1 What is DGT?

DGT, diffusive gradients in thin-films technique, was first introduced by W. Davison and Zhang (1994) as a solution device to measure trace metals in seawater. Adaption of the DGT method allows the concentration of labile metal species in aquatic systems to be measured. From a physical chemistry perspective, DGT measures analytes by allowing them to pass through a well-defined diffusion layer to a resin sink (Hartland et al., 2011). The dynamic DGT technique disturbs the equilibrium as the resin removes metal from the solution and the rate of removal is proportional to the concentration of labile metal species (Figure 6a). Theoretically, the DGT technique can be applied to determine any element or compound, providing that a selective binding agent is available and no adverse interactions between the analyte and diffusive layer are present (William Davison, 2016).

In recent years, the DGT technique has been utilised to provide information on the dissociation kinetics of various metal-ligand (ML) complexes and total metal bioavailability in natural systems. One of the advantages of DGT is that the time allowing dissociation of ML complexes is controlled by the thickness of the diffusion layer. The contribution of metal from the dissociated complex can be determined using analytical techniques (Warnken et al., 2007).

A DGT device typically comprises a binding layer and diffusive layers composed of a hydrogel and filter membrane. These layers are packed within a plastic holder with a defined “exposure window” (Figure 6b). The binding gel is covered by the hydrogel, while a filter membrane is placed on top of the hydrogel to prevent the pores clogging from particles from the environment (Ding et al., 2016). It was previously proven that the thickness of the filter membrane does not contribute significantly to the diffusion boundary layer (DBL) (W. Davison & Zhang, 1994). Therefore, the membrane is considered as part of the diffusive layer. For simplicity, the thickness of DBL (δ) is negligible when DGT is deployed in a well-stirred solution. This assumption, $\delta << \Delta g$, was validated by W. Davison and Zhang (1994), where they demonstrated that the mass of metal accumulated in the resin increased at a linear rate over time.

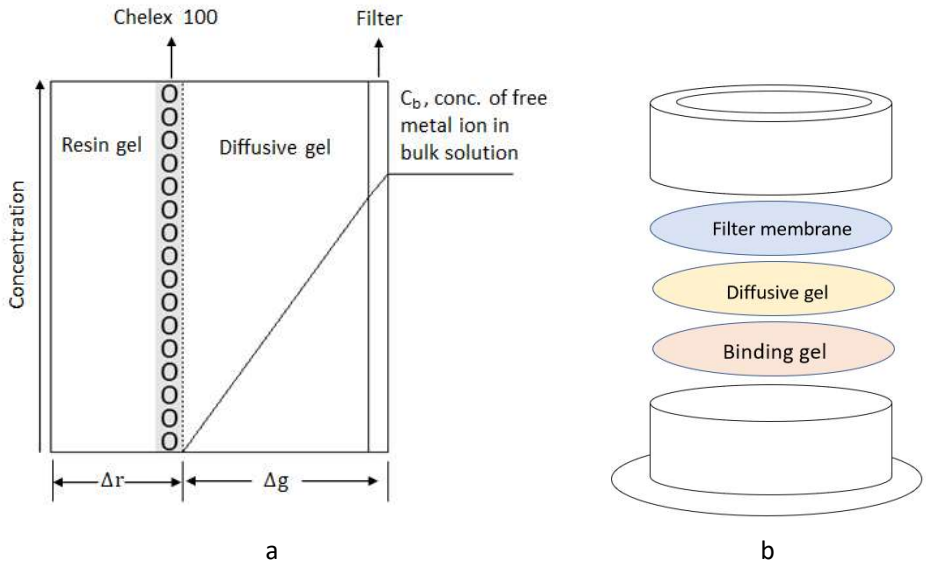


**Figure 6:** (a) the removal of free metal ions by the resin in a DGT device prevents the reformation of complexes after their dissociation and establishes a pseudo concentration gradient of complexes within the diffusive layer (Warnken et al., 2007); (b) schematic illustrations of a piston-type DGT device for deployment in solutions. The binding gel, diffusive gel and filter membrane are sequentially laid on the piston and then the ring is push-fitted over the piston base (Ding et al., 2016).

The diffusive layer permits the diffusion of solutes. The commonly used polyacrylamide hydrogel allows unimpeded diffusion of chemical species with molecular sizes smaller than the pore size of the hydrogel due to its high water content (up to 95 %) (Zhang & Davison, 1999). Diffusive properties of hydrogels are dependent on the concentration of monomer and cross-linker as well as the compositions of the ingredients. The diffusion coefficient of an individual element is also temperature dependent. In general, diffusion coefficients of common hydrogels are available from the DGT device suppliers or can be experimentally determined (Scally, Davison, & Zhang, 2006).

The binding layer absorbs the analyte(s) of interest after diffusing through the diffusive layer. It is often a thin layer of binding resin embedded in a hydrogel. For the measurement of trace metals, Chelex 100 is the preferred commercially available resin used in DGT devices (Levy, Zhang, Davison, Puy, & Galceran, 2012). The Chelex resin is a styrene-divinylbenzene co-polymer containing iminodiacetic acid (IDA) groups. It is a weak cation exchange resin that shows high affinity for divalent metal ions over monovalent ions such as potassium and sodium (Samczyński, 2006). Before the resin gel is saturated with the analyte, the concentration of the free metal ions is effectively zero as long as the equilibrium is rapid (within a few minutes) (W. Davison & Zhang, 1994).

### 3.1.2 DGT principles

Fick's first law of diffusion has been used to describe the concentration gradient in DGT.

$$F = \frac{D(C_b - C_{r)}}{\Delta g} \qquad \textit{Eq 1}$$

In which, *F* is the flux of metal ions diffusing through the diffusive layer, Δg (cm) is the thickness of the diffusive layer, *D* ($cm^2/s$) is the temperature dependent diffusion coefficient, $C_b$ *and* $C_r$ (nmol/mL) are the concentrations of labile metal species in the bulk solution and within the resin gel, respectively. As Chelex resin possesses much a stronger binding affinity to metals than ligands present in solution, the metal-resin complex forms rapidly, thus no metal ions penetrate into resin gel. $C_r$ is considered to be zero.

Flux is defined as the mass of analyte $M_a$ (nmol) that can diffuse through the effective exposure area *A* ($cm^2$) and reach the binding layer during deployment time *t* (s),

$$F = \frac{M_a A}{t} \qquad \textit{Eq 2}$$

When you combine *Eq 1* with *Eq 2*, $C_b$ can be expressed by *Eq 3*:

$$C_b = \frac{M_a \Delta g}{DAt} \qquad \textit{Eq 3}$$

$M_a$ can be determined by using *Eq 4*:

$$M_a = \frac{C_e\ (V_g + V_{acid)}}{f_e} \qquad \textit{Eq 4}$$

Where, $C_e$ (nmol/mL) is the measured concentration of the metal in the acid eluent, $V_g$ (mL) is the volume of the resin gel, $V_{acid}$ (mL) is the volume of the acid used to elute metal from resin. $f_e$ is the elution factor, which is typically 0.8 for metals bound to the Chelex resin (Zhang & Davison, 1995).

When $M_a$ is known, $C_b$ can be calculated as shown in Eq 3, providing diffusion coefficient $D$ (cm· $s^{-1}$) and DGT deployment time $t$ (s) are known. Diffusion coefficients of some species in common hydrogels are available from suppliers. Diffusion coefficients can also be determined experimentally (Scally et al., 2006).

There are implied assumptions in the DGT theory present in this work. Firstly, no ligand or complexes penetrate into the resin gel. Secondly, the ML complexes dissociate completely when they reach the binding gel. The resin binds the free metal rapidly forming a metal-resin complex which does not dissociate significantly within the time of the deployment. Finally, there is no ternary complex formed within the DGT device. The dissociation of ML complex is a first-order reaction (Shafaei Arvajeh, Lehto, Garmo, & Zhang, 2013). Species involved in this work have been simplified and represented as mobile free metal species (M), mobile free ligand (L), mobile metal-ligand complex (ML), immobile resin (R), and immobile metal-resin species (MR). The equilibrium relationships between these species are described below in Eq 5 and Eq 6:

$$\mathrm{M} + \mathrm{L} \underset{k_{diss}}{\overset{k_{form}}{\rightleftharpoons}} \mathrm{ML}$$

$$\mathrm{K_{ML}} = \frac{[\mathrm{ML}]}{[\mathrm{M}][\mathrm{L}]} = \frac{k_{form}}{k_{diss}} \qquad \text{Eq 5}$$

And,

$$M + R \underset{k_{diss\_res}}{\overset{k_{form\_res}}{\rightleftharpoons}} MR$$

$$K_{MR} = \frac{[MR]}{[M][R]} = \frac{k_{form\_res}}{k_{diss\_res}} \qquad \textit{Eq 6}$$

Where $k_{form}$ and $k_{form\_res}$ are formation rate constants ($L \cdot mol^{-1} \cdot s^{-1}$), and $k_{diss}$ and $k_{diss\_res}$ are dissociation rate constants ($s^{-1}$), $K_{ML}$ and $K_{MR}$ are the stability rate constants ($L \cdot mol^{-1}$) of the complexes. The greater the $K_{ML}$, the more stable is the ML complex (Tipping, 2002). If $K_{MR} > K_{ML}$, the resin can exchange with the ligand of the ML complex, where the ML complex is termed as "DGT labile".

As mentioned previously, the concentrations of free metal ions, free ligands and ML complexes within the DGT diffusive layer are zero before deployment. As the deployment starts, species diffuse through the hydrogel. When free metal ions and ML complexes encounter the resin, the resin sites compete with the ML. Metals are removed from weakly binding organic ligands ($L_O$) and inorganic ligands ($L_{IN}$) and adsorbed onto the resin. Hence, a diffusive gradient of metal is established. The depletion of metal leads to further dissociation of ML complex in solution, which means further supply of metal to be bound with the resin.

In summary, the exchange reactions between the DGT labile proportion of metal ($M_{DGT}$) and the ligand (L), $M_{DGT}$ and the resin (R), obey first order kinetics. The time taken to reach steady state is dependent upon the diffusion coefficients of the species and their rates of dissociation in the resin and diffusive layer. When the amount of total metal in bulk solution and that of labile metal captured by DGT

are known, the dissociation rates of the ML complexes can be mathematically inferred.

### 3.1.3 AGT: a modified form of DGT

As depicted in Figure 6, the piston-type of DGT device measures labile metal species that can diffuse through the filter membrane and diffusive gel and are bound to the resin sink. Though DGT is very useful on measuring labile complexes in natural waters. It cannot fulfil the need for characterising metal-ligand interactions in cave water studies. For example, the 'bulk solution' in a cave can be very limited (e.g. slow flow dripwaters). When measuring dripwaters from a downward growing stalactite, the DGT device must be placed under the drip point horizontally, which prevents the convective supply of solution to happen. In this instance, the metal species may precipitate on the resin gel surface regardless of their labilities.

To solve this problem, we made modifications to the DGT sampling device to directly measure the dissociation rates and determine the labilities of metal species in solution.

The design of the new device was based on another type of DGT device. Sediment probes for measurements in sediment (Figure 7) have been used to determine the flux of labile metals remobilised from the solid phase (Ding et al., 2016). Like the piston-type DGT sampler, a sediment probe consists of filter paper, chelating resin and diffusive gels packed between plastic back and front plates.

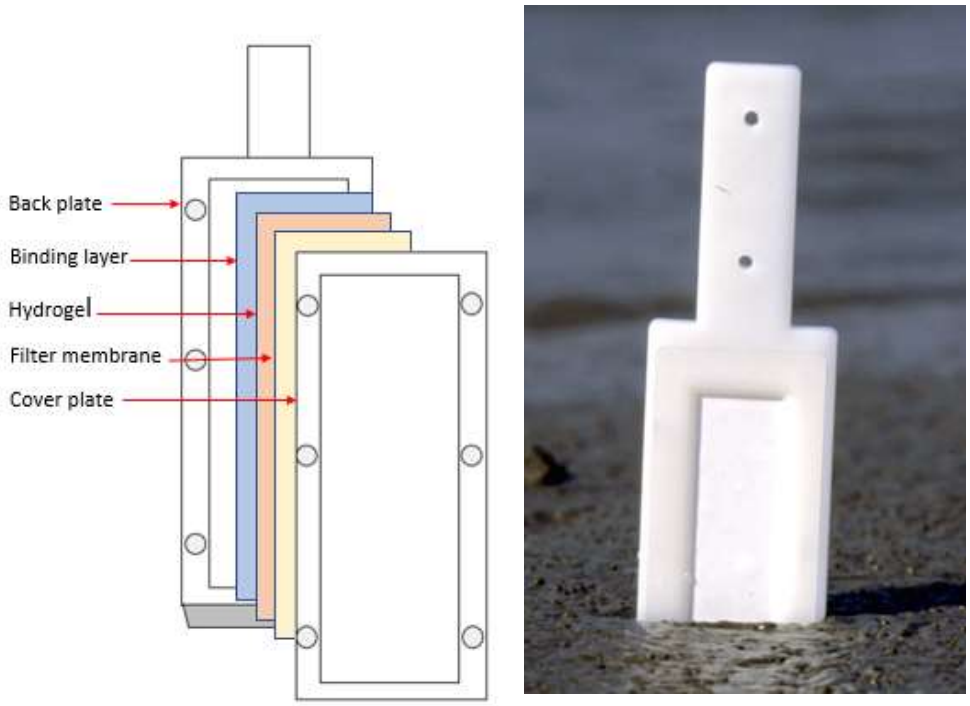


a b

**Figure 7:** (a) Schematic illustration of a sediment probe. It is a flat-type holder with a tapered end. Gel layers and filter membrane are accommodated in a base plate then sealed by a cover plate, leaving an exposure window. (b) Deployment of DGT sediment probe in soil (DGT Research Ltd, n.d.).

As this work focuses on the dissociation rates and labilities of metal-NOM complexes. The diffusion properties and behaviour of species are less significant at this stage of method development. Hence, the diffusion layer was not used throughout all experiments in this study to simplify the interpretation of results. Because the flow within the device is advective rather than diffusive, this method was labelled as advective gradients in thin-films (AGT). The modified sampling device was called the AGT channel probe.

Resin gel and filter membrane were tailored into strips with specific dimensions and packed in the AGT probe as described in section 2.2. In all experiment, the probe was positioned at a fixed 15° angle to allow test solution pass through (Figure 6c). In principle, free metal ions or metals weakly bound to ligands would be captured by the resin at the time the solution contacts the gel. In contrast, partial labile (higher binding capacity) ML complexes take longer to dissociate. Inert ML complexes dissociate at much slower rates would flow into the waste. In this model, the time available for dissociation is defined by the distance and the speed at which the flow travels. Therefore, the stronger affinity of the metal to ligand, the further down the probe the metal would be found (Figure 8).

Theoretically, only a small fraction of DGT labile metal would be adsorbed on the resin gel surface (Figure 9). The metal availability to the resin has been limited by the contact time between the flowing solution and the gel.

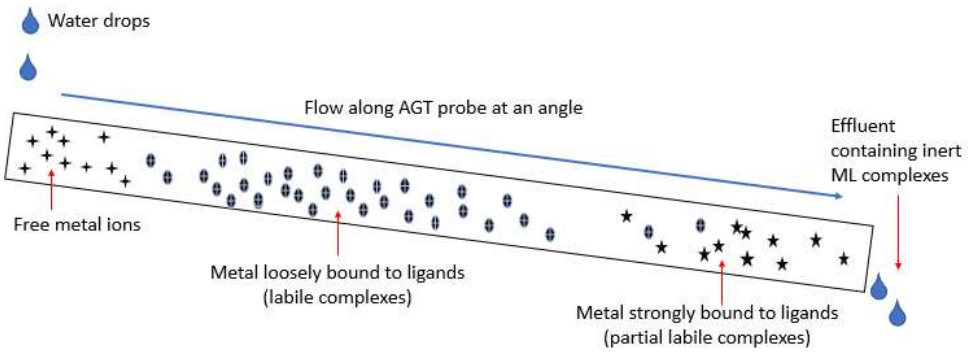


**Figure 8:** Metal-ligand complexes with various labilities dissociate at different rate. The distance the complex travels before dissociating gives information about their labilities.

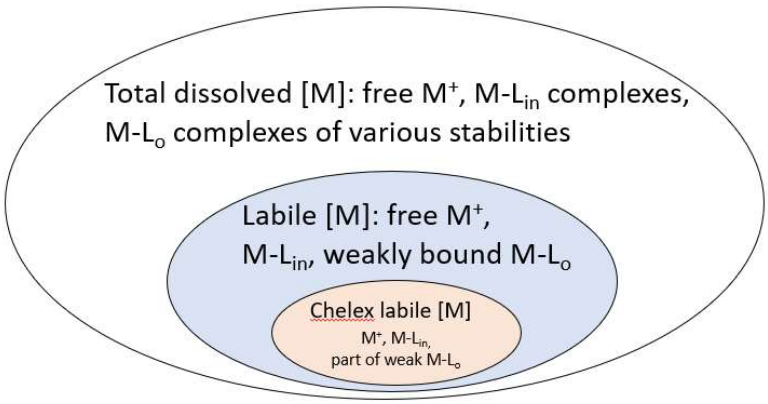


**Figure 9:** Classifications of dissolve metal species in natural waters. [M] denotes the concentration of metal.

## 3.2 Quantifying flow rate in AGT channel probe

### 3.2.1 Experimental

DI water was used as the primary water source and $Cl^-$ as the artificial tracer. Drip rates were regulated by a peristaltic pump. The unit of drip rate was "mL/min", which relates to the volume of drips that falls in 1 min. A range of drip rates (0.5 mL/min, 1 mL/min and 1.5 mL/min) were tested to establish a calibration curve. Duplicate analyses of each drip rate were carried out as a quality control procedure. The flow rate was checked at the start of each experiment.

A Chelex resin gel strip was saturated in 0.05 M NaCl solution for 4 h prior to the flow rate experiment. The assembled channel probe containing resin gel and 0.45 µm membrane filter was placed on the holder at a 15° inclination (Figure 5c). The purpose of this setting was to simulate cave water dripping conditions. Effluent samples were collected directly into the ion chromatography (IC) plastic vials, and the sampling period for each vial was 4 min long. The duration of the experiments varies from 80 – 120 min depending on the drip rate.

### 3.2.2 Results

A series of flow rate experiments were performed to calibrate the AGT probe by establishing the relationship between drip rate and flow velocity within the resin gel. Theoretically, the faster the drip rate, the higher the flow velocity within the resin gel, which manifests in the faster elution of $Cl^-$ from the AGT channel.

Data sets from the IC analysis are shown below in Figure 10, where the concentrations of $Cl^-$ have been normalised.

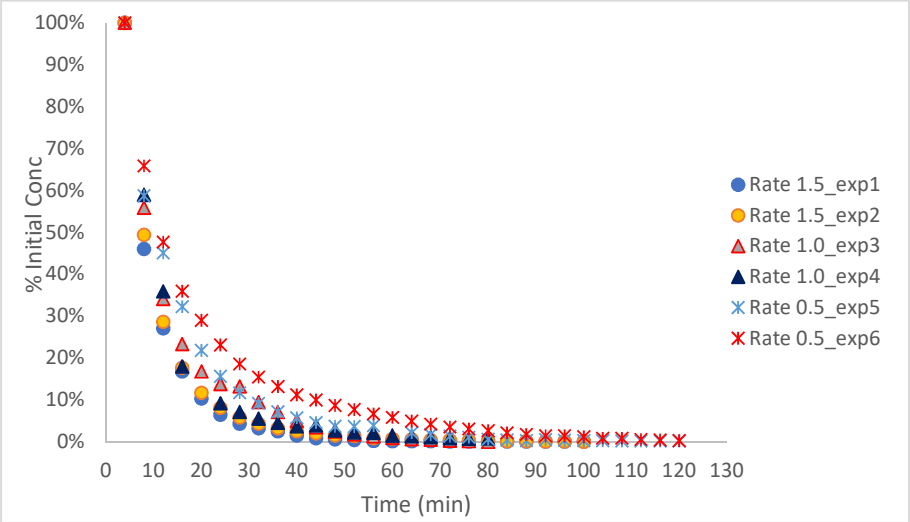


**Figure 10**: The effect of drip rates on flushing tracer out of the gel. As the drip rate increased, the flow within the gel became faster.

As the graph demonstrates, the tracer within the gel decays exponentially rather than linearly over time. Accordingly, we used the half-life of the reaction ($t_{1/2}$) to describe the decreasing rate of the tracer. Here, the half-life for one pore volume (PV) is the time to remove 50 % of the tracer. Pore volume has been used to describe the volume of a porous material. Usually, one pore volume means the liquid-filled volume of the porous material is 50 % of its total volume (1 PV % = $V_{fluid}/V_{total}$ = 50 %). In the present work, pore volume is the ratio of the removed tracer to the total amount of tracer.

The logarithmic expression of the integrated rate law for a first-order reaction is shown in *eq 7*:

$$\ln \frac{[A]}{[A]_t} = kt \qquad \text{Eq 7}$$

Where $[A]$ stands for the initial concentrations of the reactant A and $[A]_t$ for the concentration at time $t$, $k$ for the rate constant.

Fitting half of initial concentration $A_{1/2}$ and half-life time $t_{1/2}$ into the above equation, gives:

$$\ln \frac{[A]}{[A]_{1/2}} = \ln 2 = kt_{1/2} \qquad \text{Eq 8}$$

The half-life is independent of the concentration of reactants in a first order reaction. After n half-lives of a reaction, the remaining reactant is $(^1/_2)^n$ times its initial amount. Six half-lives of each experiment mean six pore volume of tracer has been flushed out of the gel, and the remaining tracer is 1.56% of its initial amount (6 PV% = $(^1/_2)^6$ = 98.44 %). The reason of using six pore volume is that most of the tracer (> 98 %) was flushed out from the gel, while the length of the experiments and the numbers of samples were experimentally acceptable.

A total of six experiments were performed with the calculated results shown below in Table 1.

**Table 1:** Summary of half-lives and flow velocities within the resin gel.

| Drip rate (ml/min) | Time to 6 PV% (min) | Averaged Time to 1 PV% (min) | Averaged Flow Velocity [b] (cm/min) |
|---|---|---|---|
| 0.5 | 70 | 13.4 | 2.24 |
| 0.5 (rpt) [a] | 91 | | |
| 1 | 54 | 9.44 | 3.18 |
| 1 (rpt) | 59 | | |
| 1.5 | 39 | 7.19 | 4.17 |
| 1.5 (rpt) | 47 | | |

a. rpt: replicate experiment

b. Flow velocity is equal to the length of gel strip (30 cm) divided by the time of 1 PV %.

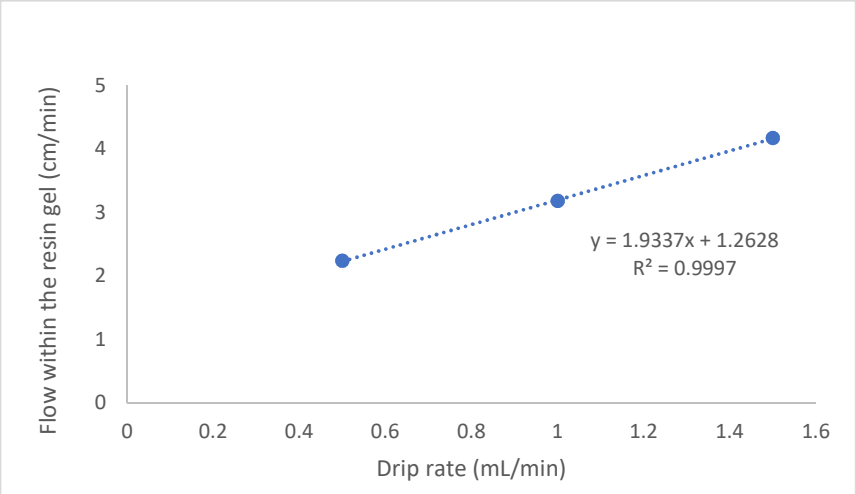


**Figure 11**: The correlation coefficients ($R^2$) of the regression were good (>99.9). A linear relationship between flow velocity within resin and drip rates proves the assumption that the faster the drip rate, the higher the flow velocity within the resin gel.

### 3.2.3 Discussion

In initial experiments, leaking from one side of the channel probe was often observed. The first version of AGT channel probe did not have the improved design of screws and holes. Initially, it was only secured by bulldog clips (Figure 12). After solution leakage between the acrylic plates was found, thread holes and nylon bolts were added into the flanks to even out the pressure along the probe (Figure 5 a& b). However, the leaking problem still occurred at the beginning of flow rate experiment. The issue may come from the horizontally tilted probe as it was mounted on a retort stand by two clamps and the solution was often found to be leaking from the thread holes on one side. To overcome this, a stand with 15° inclination made of two glass plates was constructed, which solved the problem (Figure 5c).

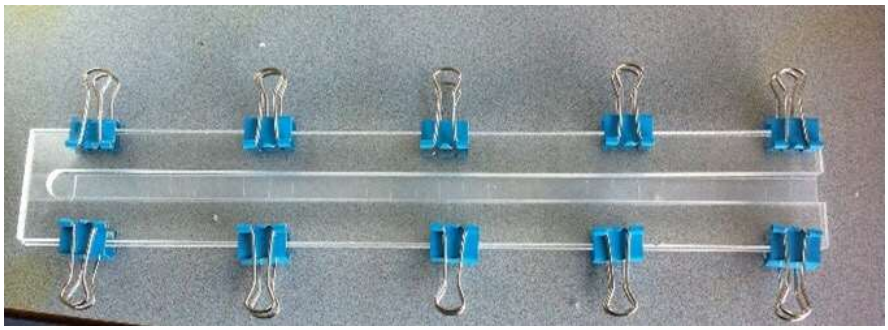

**Figure 12:** First version of the channel probe, as presented by White (2017) held together by bulldog clips.

Another problem was the poor reproducibility of results. It was thought that the inconsistent gel equilibration period was the main cause of the problem. The preparations include soaking resin gel strip in 0.05 M NaCl to saturate the gel with tracer $Cl^-$.

In the first version of the experimental procedure, the saturating period was 24 h. In fact, the length of time was not controlled at exact 24 h but with ~3 h deviation (i.e. 21-27 h).

The results showed that the longer the resin gel was soaked in NaCl, the more Cl- was concentrated in the resin as a higher level of $Cl^-$ in the first sample vial was detected.

In order to minimise the variations due to soaking time, the saturating period was shortened to 4 h, which is more practical. The excessive NaCl solution was drained after the resin gel was placed in the probe to avoid artificially high $Cl^-$ in the first few samples.

As presented in Table 1, better precision was attained at higher drip rates. However, it was expected that at lower drip rates, the measured time of six pore

volume would have a greater difference between duplicate experiments. Due to the imperfect resin gel fabricating method, Chelex resin cannot be distributed homogeneously over the whole gel sheet. Because of this, it was difficult to obtain a 30 cm long strip with evenly distributed resin beads. This would contribute to poorly interconnected and more diluted pores on part of the gel strip. When this happens, the gel acts as a diffusive layer rather as a binding layer. Tracers penetrate into this part of the gel and are removed slower than the rest of the system (White, 2017). Consequently, when the source solution drips at lower rates, the residence time on the gel is longer. Hence, more tracers would be flushed out and collected in sample vials, resulting in a higher $Cl^-$ concentration. To identify and potentially minimise this bias, replicate experiments should be carried out to evaluate the quality of the gel based on its reproducibility.

## 3.3 Measuring dissociation rate of known metal-ligand complex

### 3.3.1 Experimental

The channel probe was assembled and set up using the same protocol for the previous flow rate experiment. The Chelex resin gel strip was stored in 0.01 M $NaNO_3$ to maintain a stable dimension, and the filter membrane was hydrated in DI water before use. When the Chelex resin gel is equilibrated with $NaNO_3$ solution, all the binding sites of the absorbent are occupied by the easily exchangeable sodium ions ($Na^+$). As soon as the experiment begins and the test solution passes through the resin gel, the sodium ions are exchanged by nickel ions ($Ni^{2+}$) with higher affinity for the Chelex resin (William Davison, 2016).

Due to the low metal concentration and the complexity of organic matter present in natural waters, synthetic solutions containing known metal and organic ligand were chosen to be investigated in this section. The test solutions were prepared based on the method given by Shafaei Arvajeh et al. (2013) but with modifications of pH and metal to ligand ratios. A phosphate buffer at pH 8.0 ± 0.2 was prepared by mixing 53 mL of 0.01 M $Na_2HPO_4$ and 947 mL of 0.01 M $NaH_2PO_4$. Freshly prepared pH 8.0 phosphate solution was used to prepare a nitrilotriacetic acid (NTA) stock solution, as NTA readily dissolves in basic solution. All deployment solutions gave final concentrations of 0.01 M $NaNO_3$ and 0.01 M phosphate salts. The compositions of test solutions are listed in Table 2. A quality control solution D for testing method performance was comprised of only free $Ni^{2+}$. All solutions were left to equilibrate for 24 h before use.

**Table 2:** Compositions of solutions used in the metal experiment

| Test Solution Compositions | | | | 1000 µg/mL Ni stock | 1000 µg/mL NTA stock | Final Vol. [a] |
|---|---|---|---|---|---|---|
| Experiment# | Ni (µM) | NTA (µM) | M:L ratio | (mL) | (mL) | (L) |
| A | 100 | 200 | 0.5 | 2.94 | 19.1 | 0.5 |
| B | 50 | 200 | 0.25 | 1.47 | 19.1 | 0.5 |
| C | 25 | 200 | 0.125 | 0.74 | 19.1 | 0.5 |
| D | 25 | 0 | N/A [b] | 0.74 | 0 | 0.5 |

a. Make up to final volume with pH 8.0 phosphate buffer solution.

b. N/A: not applicable

Before the start and at the end of each experiment, 10 mL of test solution from the reservoir and effluent from the probe were taken as reference solutions. Temperature, pH, conductivity and the concentrations of metal ions were all measured. For ICP-MS analysis, 0.1 mL of concentrated $HNO_3$ was added into 5 mL of each reference solution to produce a sample matrix with 2 % $HNO_3$ for ICP-MS analysis. The drip rate for this set of experiments was set at 1 ± 0.05 mL/min.

All experiments had a five-hour deployment time. Upon completion of the deployment, the resin gel strip was dissected at 1 cm interval and transferred into a set of 15 mL polypropylene tubes containing 1 mL of 1 M $HNO_3$. It is important to avoid stretching the gel strip when transferring from the probe to the chopping board. This was done by using two pairs of forceps to lift both ends of the filter membrane and resin gel (as a whole) up, and then placing it gently on the board.

Once successfully transferred, the filter membrane was peeled off, and the gel was cut at 1 cm intervals. The gel slices were numbered according to their distance away from the drip point (Figure 13).

Thirteen representative samples (highlighted in yellow in Figure 13) were selected for ICP- MS analysis while the rest of them were archived for future analysis. 1 mL of 1 M $HNO_3$ was added into each sample tube to elute nickel bound by the Chelex resin. After 48 h extraction, each eluate was diluted with 4 mL of DI water, and the supernatant (resin free) was taken for ICP-MS analysis.

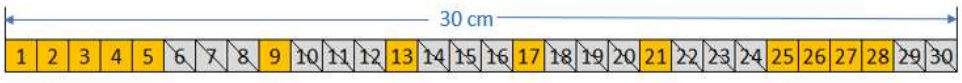


**Figure 13:** Labelling of resin gel sample from the drip point.

### 3.3.2 Results

The final pH of all deployment solutions varied from 7.51 to 7.90, while the conductivity ranged from 2.31 mS/m to 2.62 mS/m. All measurements were conducted at a controlled laboratory temperature of 20 °C.

The application of the equilibrium speciation program Visual MINTEQ version 3.1 has helped to understand nickel speciation in deployment solutions. The concentration of components in experimental solutions, along with other parameters are listed in Table 3. These units were input into the program to calculate the distribution of nickel species.

**Table 3**: Visual MINTEQ input data

| | | | Concentration (µg/mL) | | | | |
|---|---|---|---|---|---|---|---|
| Exp# | pH [a] | Temp °C | $Ni^{2+}$ | $NTA^{3-}$ | $Na^{+}$ | $NO_3^{-}$ | $PO_4^{3-}$ |
| A | 7.51 | 20.4 | 5.87 | 38.23 | 677.91 | 620 | 949.714 |
| B | 7.77 | 21.6 | 2.93 | 38.23 | 677.91 | 620 | 949.714 |
| C | 7.86 | 19.8 | 1.47 | 38.23 | 677.91 | 620 | 949.714 |
| D | 7.90 | 20.0 | 1.47 | n/a | 677.91 | 620 | 949.714 |

a. Measured pH after 24 h equilibration

**Table 4:** Visual MINTEQ output data

| Exp# | Ionic strength | % species | | | | |
|---|---|---|---|---|---|---|
| | | $NiNTA^-$ | $Ni(NTA)^{(2-4)+}$ | $NiOHNTA^{2-}$ | $Ni^{2+}$ | $(aq)NiHPO_4$ |
| A | 0.0346 | 98.362 | 1.615 | 0.022 | n/a | n/a |
| B | 0.0357 | 95.637 | 4.322 | 0.041 | n/a | n/a |
| C | 0.0361 | 93.812 | 6.141 | 0.046 | n/a | n/a |
| D | 0.0358 | n/a | n/a | n/a | 38.459 | 60.751 |

The resulting Visual MINTEQ output data is tabulated in Table 4. When the organic ligand NTA was present in solution A/B/C, $NiNTA^-$ is the dominant species (>99.3 %) at equilibrium. Also, Ni-NTA complexes accounted for more than 99.9 % of total nickel in these three solutions. Solution D was the control solution to simulate nickeel accumulation in the absence of organic ligand. Nickel ions and dissolved NiHPO4 were the major metal species determined (>99.2 %), which are fully labile to the Chelex resin.

The experimental results for nickel adsorbed on Chelex resin as a function of distance is plotted in Figure 14. The mass of nickel accumulated on one Chelex resin gel slice was calculated by *eq 4*, given in section 3.1.2.

According to the Visual MINTEQ prediction, free nickel ions in solution A/B/C would be rapidly removed. Therefore, we treated the initial 5 cm of the gel as an 'equilibration zone'. Nickel accumulation at a distance of 5 to 25 cm was considered to be more representative for estimating dissociation rates of Ni-NTA complexes (shown in Figure 15). Nickel concentrations in the experiments

decrease monotonically in the centre part of the probe, consistent with well-defined, dissociation-controlled rates in this region.

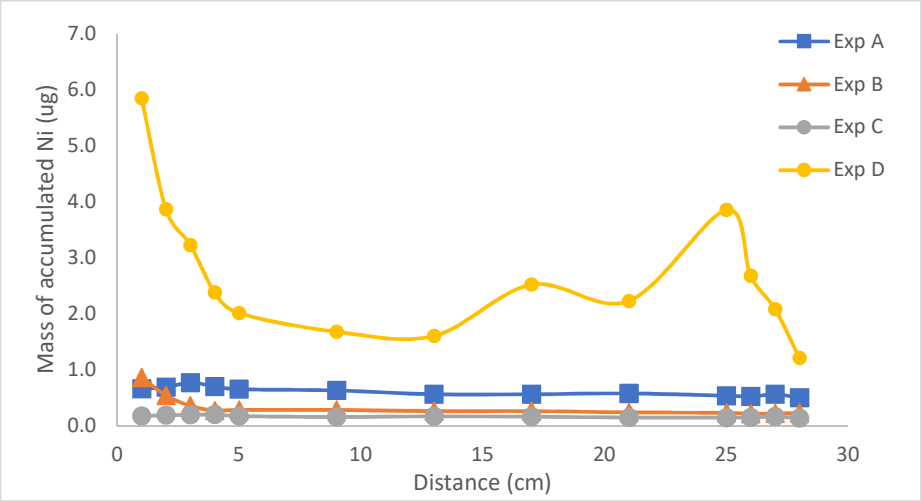


**Figure 14:** Metal accumulation curves from the four metal accumulation experiments.

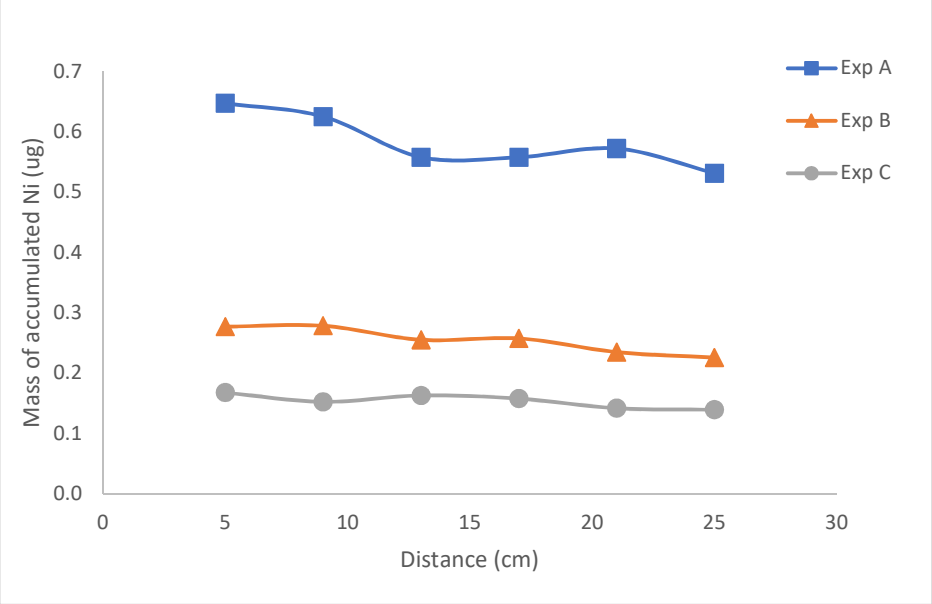


**Figure 15:** The distance from 5 cm to 25 cm is a more representative zone in terms of slow dissociation of Ni-NTA complexes.

### 3.3.3 Discussion

The initial rapid deletion of nickel in experiment D shown in Figure 14 is consistent with the prediction that free metal ions and fully labile inorganic complexes would be removed from the solution once they encounter the Chelex resin. However, the increase in accumulated nickel at the far end of the gel highlights the frailty of this method, which could lead to larger experimental errors. In section 3.2.3, the inhomogeneous distribution of the resin beads over the gel was previously discussed, along with the potential effect of producing unwanted divergences in flow rate and residence time, hence nickel accumulation. It is worth mentioning that when assembling the channel probe, the end of the gel with more densely packed Chelex beads was always placed at the head of the probe (under the drip point) to improve the reproducibility. This would have contributed to the curve observed for experiment D in Figure 14.

The data sets of experiment A/B/C indicate that the fraction of nickel bound to resin decreases with decreasing ratios of nickel to NTA (from 0.5 to 0.125). Shafaei Arvajeh et al. (2013) used standard piston-like DGT devices to measure Ni-NTA complexes in synthetic solutions for a period of 24 h. One of their findings is that only 20 – 26 % of the total Ni-NTA complexes in the solutions contribute to the mass of nickel bound by Chelex resin. The implication to our study is that only a fraction of Ni-NTA complexes can dissociate and are adsorbed onto the resin gel during the flow residence time (see Figure 9). These findings were confirmed by the results presented in the forward modelling with three metal experiment data sets (see Appendix IV). The calculated percentage of Chelex-labile nickel in

solutions with different concentration of total nickel ranged from 0.26 % to 0.35 %, with an acceptable relative standard deviation of 9.0 %. Note that the details of the accumulation modelling are not presented here as they are the work of Dr Hartland.

The mean value of 0.32% representing the Chelex-labile fraction of nickel , and a mean dissociation rate at $2.0 \times 10^4\ s^{-1}$ (Shafaei Arvajeh et al., 2013) were used in the forward modelling of metal accumulation experiments. The theoretical mass of nickel bound to resin gel slices in all three experiments wererelatively consistent with the measured values, after taking the experiment errors into consideration.

Improvements with gel preparation procedures and the whole AGT probe related device are recommended. The operator-related error will be minimised when the quality of gel sheet and device set-up become more reproducible.

## 3.4 Deployment of AGT in the Cave

### 3.4.1 Study site

Aranui Cave (38.2651° S, 175.0796° E), is in the Waitomo District on the North Island of New Zealand, about 75 km away from The University of Waikato. This region consists of a limestone karst landscape which was lifted out of the sea as the result of tectonic activities. Aranui cave is part of the Waitomo caves system and among the few commercial caves that are famous for their cave formations (Waitomo Caves, 2013).

Situated in the centre of the North Island, Waitomo region has wet winters and warm summers. According to the information provided by Waitomo District Council in 2019, the mean temperature ranges from 18.5 °C in summer to 9.5 °C in winter, while mean annual precipitation was about 1473 mm.

### 3.4.2 Experiment

An active speleothem-forming drip point with relatively fast drip rate was identified for AGT channel probe deployment (Figure 16a). The channel probe remained in situ for a total of 17 days and 0.5 hours during early Autumn (10:00 am, 8$^{th}$ March – 10:30 am, 24$^{th}$ March 2019).

The average drip rates were 1’45’’/drip measured on 8$^{th}$ March and 1’30’’/drip measured on 25$^{th}$ March. One drip water sample was also collected into an acid-cleaned polyethylene tube directly from the same actively-depositing stalactite (Figure 16b) after the withdrawal of the AGT channel probe. Approximately 20 mL of dripwater sample was collected in 3.75 h (10:30 am – 2:15 pm, 24$^{th}$ March 2019).

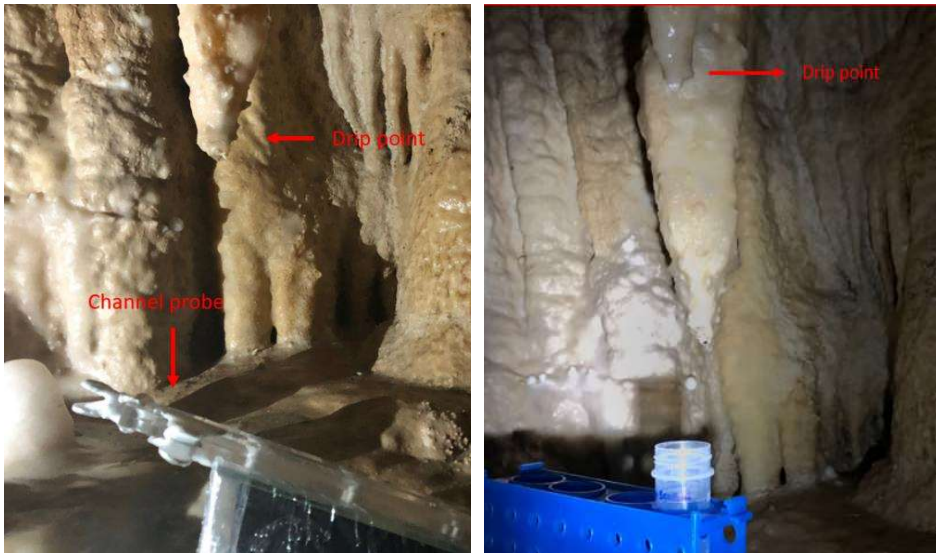


a b

**Figure 16:** (a) Deployment of channel probe in Aranui Cave, Waitomo. (b) Sampling the speleothem-forming dripwaters from the same stalactite.

The channel probe was placed into a clean laboratory sample bag and transferred back to the laboratory at The University of Waikato on the same day followed by extraction procedures. The pH 7.28 at 17.8 °C of the unfiltered sample was also measured.

As previously described in the metal accumulation experiment (section 3.3.1), the resin gel strip was removed from the probe and divided into 1 cm slices. All gel slices were stored in labelled 15 mL falcon tubes separately. Bound metals were eluted with the addition of 1 M $HNO_3$ as previously described.

### 3.4.3 Result

The first twelve gel segments (1 – 12 cm) and one drip water sample were taken for ICP-MS analysis. Transition metals were of interest due to their strong binding

affinities to NOM. Most of these metals, including nickel, were not found in either the drip water sample or resin gel samples. However, four transition metals (copper, zinc, chromium, yttrium) were detected, and these are discussed further below.

An average drip rate of 1.624 min/drip was used to estimate the amount of drip water passed through the channel probe. As 20 mL of drip water was collected in 225 min, the mean volume per drip is 0.144 mL. Therefore, in 17 days and 0.5 hours, a total of 2.18 L of drip water was measured in situ by this AGT method.

It was found that only a small fraction (average 0.32 %) of total nickel was able to dissociate from ML complexes in the metal accumulation experiment using synthetic metal-organic ligand solutions. From the cave results, 0.11 % -2.47 % of the total transition metals was adsorbed onto the resin gel. The behaviour of the four detected metals above detection limits forming complexes of unknown labilities is shown in Figure 17.

a

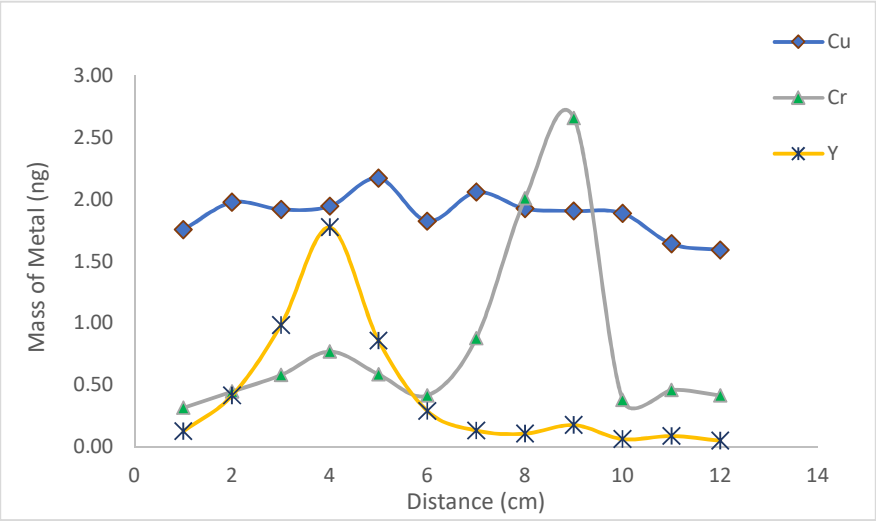


b

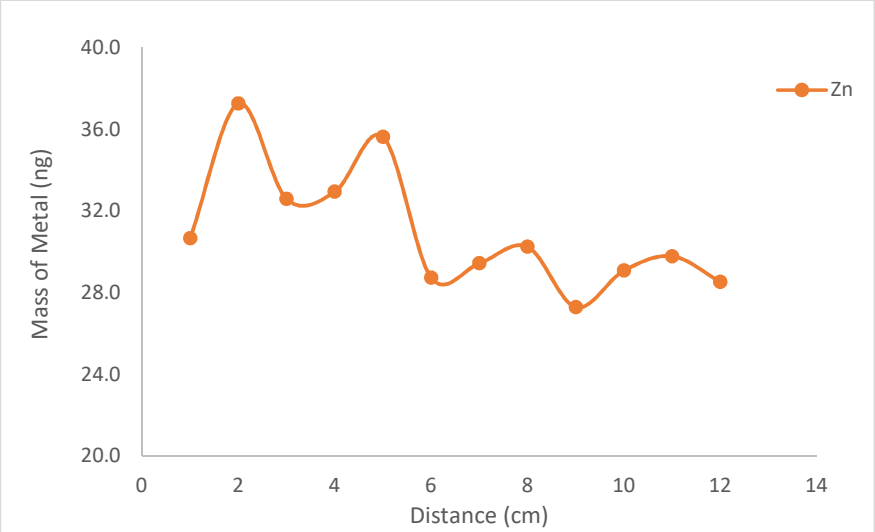


**Figure 17:** Metal accumulation behaviour from 1 to 12 cm of the cave dripwater exposed gel strip for a) copper, chromium and yttrium, and b) zinc.

### 3.4.4 Discussion

The accumulation curves in Figure 17 demonstrated the ability of AGT method reflecting the labilities of metal-NOM complexes from the distance that the maximum amount of metal accumulated. NOM complexing parameters for chromium and yttrium are scarce in the literature. Therefore, we were only able

to compare the labilities of Cr-NOM and Y-NOM complexes in this study, as they had similar accumulation patterns in the field experiment. The greatest Cr-NOM complexes dissociated at a further distance (9 cm) than the Y-NOM complexes (4 cm). From this result, it can be inferred that the Cr-NOM complexes presented higher binding strengths than the Y-NOM complexes.

The fluctuating trend of Chelex labile fraction of copper (Figure 17a) indicated the high stability of Cu-NOM complexes. Moreover, the dissociation behaviour of copper showed no significant difference over the first 12 cm of the resin gel. A possible explanation for this observation is that the depletion of copper from the flow in the first 12 cm distance was incomplete and that the deletion of this metal may occur in subsequent gel segments (e.g. 13 to 30 cm), unless Cu-NOM complexes present in the measured dripwaters were inert to the Chelex resin.

Interestingly, the dissociation behaviour of zinc suggested that there are ligands with various binding strengths to zinc present in the dripwaters. Two weakly bound Zn-NOM complexes were observed that dissociated rapidly and giving two equivalent peaks at a distance of 2 cm and 5 cm.

Based on these results, the observed binding affinities to NOM between these four metals, from highest to lowest, follow the order Cu > Cr > Y > Zn. This finding is supported by the results presented by Warnken et al. (2007), where zinc complexes had a slower dissociation rate constant than copper. According to the Eigen mechanism, the dissociation rates for the metal-ligand complexes are inversely proportional to the stability constant of the complex. Therefore, complexes with copper species have higher stabilities than zinc-ligand complexes, which is consistent with the order listed above.

# Chapter 4 Conclusion

Overall, the AGT method was able to generate results consistent with our initial assumptions (see section 3.1.3). The results from reverse modelling (see Appendix III) show that the predicted concentrations of total nickel in effluent have very little difference (3.2 % ~ 4.5 %) with the measured values. We also used the mean dissociation rate for Ni-NTA complexes from the literature to estimate the amount of nickel accumulated on Chelex resin, which is called forward modelling. The predicted values were also found to be in good agreement with the measured values (see Appendix IV), confirming the accuracy of the theoretical modelling.

This study investigated not only the practicality of the AGT channel probe method, but also its ability to directly measure unknown metal-ligand complexes in cave waters. The advantages of this method are that the data can provide distinguishable patterns of metal accumulation, and the dissociation rates of the ML complexes can be mathematically solved without knowing the actual composition of the ligands.

This pilot study clearly demonstrated that both the calibration of the AGT device and the interpretation of the in situ measurements are work in progress. Improvements are required to achieve resin gel consistency. It will also be necessary to carry out additional measurements on the same metal (nickel) with other well-characterised organic ligands such as FA and HA to fully validate the AGT method.

# References


1. Borsato, A., Frisia, S., Fairchild, I. J., Somogyi, A., & Susini, J. (2007). Trace element distribution in annual stalagmite laminae mapped by micrometer-resolution X-ray fluorescence: Implications for incorporation of environmentally significant species. *Geochimica et Cosmochimica Acta, 71*(6), 1494-1512. https://doi.org/https://doi.org/10.1016/j.gca.2006.12.016

2. Cruz, F. W., Burns, S. J., Jercinovic, M., Karmann, I., Sharp, W. D., & Vuille, M. (2007). Evidence of rainfall variations in Southern Brazil from trace element ratios (Mg/Ca and Sr/Ca) in a Late Pleistocene stalagmite. *Geochimica et Cosmochimica Acta, 71*(9), 2250-2263. https://doi.org/http://doi.org/10.1016/j.gca.2007.02.005

3. Davison, W. (2016). *Diffusive Gradients in Thin-Films for Environmental Measurements*. Cambridge, England: Cambridge University Press.

4. Davison, W., & Zhang, H. (1994). In-situ speciation measurements of trace components in natural waters. *Nature, 367*(2), 546-548.

5. DGT Research Ltd. (n.d.). *LSPM-NP Loaded DGT device for metals (A) in sediment.* Retrieved from https://www.dgtresearch.com/product/lspm-loaded-dgt-device-for-metals-a-in-sediment/

6. Ding, S., Wang, Y., Zhang, L., Xu, L., Gong, M., & Zhang, C. (2016). New holder configurations for use in the diffusive gradients in thin films (DGT) technique. *RSC Advances, 6*(91), 88143-88156. https://doi.org/10.1039/c6ra19677b

7. Fairchild, I. J., Borsato, A., Tooth, A. F., Frisia, S., Hawkesworth, C. J., Huang, Y., . . . Spiro, B. (2000). Controls on trace element (Sr–Mg) compositions of carbonate cave waters: implications for speleothem climatic records. *Chemical Geology, 166*(3), 255-269. https://doi.org/http://doi.org/10.1016/S0009-2541(99)00216-8

8. Fairchild, I. J., Smith, C. L., Baker, A., Fuller, L., Spötl, C., Mattey, D., . . . E.I.M.F. (2006). Modification and preservation of environmental signals in speleothems. *Earth-Science Reviews, 75*(1), 105-153. https://doi.org/https://doi.org/10.1016/j.earscirev.2005.08.003

9. Fairchild, I. J., & Treble, P. C. (2009). Trace elements in speleothems as recorders of environmental change. *Quaternary Science Reviews, 28*(5), 449-468. https://doi.org/https://doi.org/10.1016/j.quascirev.2008.11.007

10. Genty, D., Baker, A., & Vokal, B. (2001). Intra- and inter-annual growth rate of modern stalagmites. *Chemical Geology, 176*(1), 191-212. https://doi.org/https://doi.org/10.1016/S0009-2541(00)00399-5

11. Hartland, A., Fairchild, I. J., Lead, J. R., Zhang, H., & Baalousha, M. (2011). Size, speciation and lability of NOM–metal complexes in hyperalkaline cave dripwater. *Geochimica et Cosmochimica Acta, 75*(23), 7533-7551. https://doi.org/10.1016/j.gca.2011.09.030

12. Hellstrom, J. C., & McCulloch, M. T. (2000). Multi-proxy constraints on the climatic significance of trace element records from a New Zealand speleothem. *Earth and Planetary Science Letters, 179*(2), 287-297. https://doi.org/http://doi.org/10.1016/S0012-821X(00)00115-1

13. Johnson, K. R., Hu, C., Belshaw, N. S., & Henderson, G. M. (2006). Seasonal trace-element and stable-isotope variations in a Chinese speleothem: The potential for high-resolution paleomonsoon reconstruction. *Earth and Planetary Science Letters, 244*(1), 394-407. https://doi.org/https://doi.org/10.1016/j.epsl.2006.01.064

14. Kalis, E. J. J., Weng, Dousma, F., Temminghoff, E. J. M., & Van Riemsdijk, W. H. (2006). Measuring free metal ion concentrations in situ in natural waters using the donnan membrane technique. *Environmental Science and Technology, 40*(3), 955-961. https://doi.org/http://doi.org/10.1021/es051435v

15. Lee, Y. J., Elzinga, E. J., & Reeder, R. J. (2005). Cu(II) adsorption at the calcite–water interface in the presence of natural organic matter: Kinetic studies and molecular-scale characterization. *Geochimica et Cosmochimica Acta, 69*(1), 49-61. https://doi.org/http://doi.org/10.1016/j.gca.2004.06.015

16. Lehto, N. J. (2016). *Handout - Preparing and testing DGT probes* NZ

17. Levy, J. L., Zhang, H., Davison, W., Puy, J., & Galceran, J. (2012). Assessment of trace metal binding kinetics in the resin phase of diffusive gradients in thin films. *Analytica Chimica Acta, 717*, 143-150. https://doi.org/http://doi.org/10.1016/j.aca.2011.12.043

18. McDermott, F. (2004). Palaeo-climate reconstruction from stable isotope variations in speleothems: a review. *Quaternary Science Reviews, 23*(7), 901-918. https://doi.org/http://doi.org/10.1016/j.quascirev.2003.06.021

19. McKnight, D. M., Hornberger, G. M., Bencala, K. E., & Boyer, E. W. (2002). In‐stream sorption of fulvic acid in an acidic stream: A stream‐scale transport experiment. *Water Resources Research, 38*(1), 6-1-6-12. https://doi.org/http://doi.org/10.1029/2001WR000269

20. Richards, D. A., & Dorale, J. A. (2003). Uranium-series chronology and environmental applications of speleothems. *Reviews in Mineralogy and Geochemistry, 52*(1), 407-460. https://doi.org/https://doi.org/10.2113/0520407

21. Samczyński, Z. (2006). Ion exchange behavior of selected elements on Chelex 100 resin. *Solvent Extraction and Ion Exchange, 24*(5), 781-794. https://doi.org/http://doi.org/10.1080/07366290600846174

22. Scally, S., Davison, W., & Zhang, H. (2006). Diffusion coefficients of metals and metal complexes in hydrogels used in diffusive gradients in thin films. *Analytica Chimica Acta, 558*(1), 222-229. https://doi.org/http://dx.doi.org/10.1016/j.aca.2005.11.020

23. Scroxton, N., Burns, S., Dawson, P., Rhodes, J. M., Brent, K., McGee, D., . . . Gagan, M. (2018). Rapid measurement of strontium in speleothems using core-scanning micro X-ray fluorescence. *Chemical Geology, 487*, 12-22. https://doi.org/http://doi.org/10.1016/j.chemgeo.2018.04.008

24. Shafaei Arvajeh, M. R., Lehto, N., Garmo, Ø. A., & Zhang, H. (2013). Kinetic studies of Ni organic complexes using diffusive gradients in thin films (DGT) with double binding layers and a dynamic numerical model. *Environmental Science and Technology, 47*(1), 463-470. https://doi.org/http://doi.org/10.1021/es301371b

25. Sigg, L., Black, F., Buffle, J., Cao, J., Cleven, R., Davison, W., . . . Zhang, H. (2006). Comparison of analytical techniques for dynamic trace metal speciation in natural freshwaters. *Environmental Science and Technology, 40*(6), 1934-1941. https://doi.org/http://doi.org/10.1021/es051245k

26. Tipping, E. (2002). *Cation binding by humic substances*. Cambridge, England: Cambridge University Press.

27. Treble, P., Shelley, J. M. G., & Chappell, J. (2003). Comparison of high resolution sub-annual records of trace elements in a modern (1911–1992) speleothem with instrumental climate data from southwest Australia. *Earth and Planetary Science Letters, 216*(1), 141-153. https://doi.org/10.1016/S0012-821X(03)00504-1

28. Unsworth, E. R., Warnken, K. W., Zhang, H., Davison, W., Black, F., Buffle, J., . . . Xue, H. (2006). Model predictions of metal speciation in freshwaters compared to measurements by in situ techniques. *Environmental Science and Technology, 40*(6), 1942-1949. https://doi.org/10.1021/es051246c

29. van Beynen, P. E., Schwarcz, H. P., Ford, D. C., & Timmins, G. T. (2002). Organic substances in cave drip waters: studies from Marengo Cave, Indiana. *Canadian Journal of Earth Sciences, 39*(2), 279-284. https://doi.org/10.1139/e01-072

30. Waitomo Caves. (2013). *Waitomo Caves Geology.* Retrieved from http://www.waitomo-caves.com/about-waitomo-caves/Waitomo-caves-geology/

31. Warnken, K. W., Davison, W., & Zhang, H. (2008). Interpretation of in situ speciation measurements of inorganic and organically complexed trace metals in freshwater by DGT. *Environmental Science and Technology, 42*(18), 6903-6909. https://doi.org/http://doi.org/10.1021/es800359n

32. Warnken, K. W., Davison, W., Zhang, H., Galceran, J., & Puy, J. (2007). In situ measurements of metal complex exchange kinetics in freshwater. *Environmental Science and Technology, 41*(9), 3179-3185. https://doi.org/http://doi.org/10.1021/es062474p

33. White, J. (2017). DGT probe preparation SOP_Jackson 2017Aug.

34. Waitomo District Council (2019). *Your District.* Retrieved from http://www.waitomo.govt.nz/council/our-place/

35. Zhang, H., & Davison, W. (1995). Performance characteristics of diffusion gradients in thin films for the in situ measurement of trace metals in aqueous solution. *Analytical Chemistry, 67*(19) https://doi.org/http://doi.org/10.1021/ac00115a005,

36. Zhang, H., & Davison, W. (1999). Diffusional characteristics of hydrogels used in DGT and DET techniques. *Analytica Chimica Acta, 398*(2–3), 329-340. https://doi.org/https://doi.org/10.1016/S0003-2670(99)00458-4

# Appendices

## Appendix I: Analysis of Flow Rate Experiment Data

**Table 5:** IC raw data collected from flow rate experiment 1

| Deployment Time (min) | Exp#_DripRate_Vial ID | Chloride Amount (mg/L) | Normalised Concentration |
|---|---|---|---|
| 4 | Exp 1_Rate 1.5_pos#1 | 275.6727 | 100.00% |
| 8 | Exp 1_Rate 1.5_pos#2 | 126.7936 | 45.99% |
| 12 | Exp 1_Rate 1.5_pos#3 | 74.4717 | 27.01% |
| 16 | Exp 1_Rate 1.5_pos#4 | 46.2396 | 16.77% |
| 20 | Exp 1_Rate 1.5_pos#5 | 28.5092 | 10.34% |
| 24 | Exp 1_Rate 1.5_pos#6 | 17.6832 | 6.41% |
| 28 | Exp 1_Rate 1.5_pos#7 | 11.8483 | 4.30% |
| 32 | Exp 1_Rate 1.5_pos#8 | 8.9292 | 3.24% |
| 36 | Exp 1_Rate 1.5_pos#9 | 6.8706 | 2.49% |
| 40 | Exp 1_Rate 1.5_pos#10 | 4.0389 | 1.47% |
| 44 | Exp 1_Rate 1.5_pos#11 | 2.2356 | 0.81% |
| 48 | Exp 1_Rate 1.5_pos#12 | 1.5536 | 0.56% |
| 52 | Exp 1_Rate 1.5_pos#13 | 1.0766 | 0.39% |
| 56 | Exp 1_Rate 1.5_pos#14 | 0.6484 | 0.24% |
| 60 | Exp 1_Rate 1.5_pos#15 | 0.3334 | 0.12% |
| 64 | Exp 1_Rate 1.5_pos#16 | 0.3243 | 0.12% |
| 68 | Exp 1_Rate 1.5_pos#17 | 0.2984 | 0.11% |
| 72 | Exp 1_Rate 1.5_pos#18 | 0.1897 | 0.07% |
| 76 | Exp 1_Rate 1.5_pos#19 | 0.1756 | 0.06% |
| 80 | Exp 1_Rate 1.5_pos#20 | 0.1810 | 0.07% |
| 84 | Exp 1_Rate 1.5_pos#21 | 0.1150 | 0.04% |
| 88 | Exp 1_Rate 1.5_pos#22 | 0.1519 | 0.06% |
| 92 | Exp 1_Rate 1.5_pos#23 | 0.1232 | 0.04% |
| 96 | Exp 1_Rate 1.5_pos#24 | 0.1311 | 0.05% |
| 100 | Exp 1_Rate 1.5_pos#25 | 0.0997 | 0.04% |

**Table 6:** IC raw data collected from flow rate experiment 2

| Deployment Time (min) | Exp#_DripRate_Vial ID | Chloride Amount (mg/L) | Normalised Concentration |
|---|---|---|---|
| 4 | Exp 2_Rate 1.5_pos#1 | 278.2812 | 100.00% |
| 8 | Exp 2_Rate 1.5_pos#2 | 137.4272 | 49.38% |
| 12 | Exp 2_Rate 1.5_pos#3 | 79.6688 | 28.63% |
| 16 | Exp 2_Rate 1.5_pos#4 | 49.1765 | 17.67% |
| 20 | Exp 2_Rate 1.5_pos#5 | 32.4976 | 11.68% |
| 24 | Exp 2_Rate 1.5_pos#6 | 22.4843 | 8.08% |
| 28 | Exp 2_Rate 1.5_pos#7 | 16.1279 | 5.80% |
| 32 | Exp 2_Rate 1.5_pos#8 | 11.9647 | 4.30% |
| 36 | Exp 2_Rate 1.5_pos#9 | 8.9641 | 3.22% |
| 40 | Exp 2_Rate 1.5_pos#10 | 6.8667 | 2.47% |
| 44 | Exp 2_Rate 1.5_pos#11 | 5.5337 | 1.99% |
| 48 | Exp 2_Rate 1.5_pos#12 | 4.0932 | 1.47% |
| 52 | Exp 2_Rate 1.5_pos#13 | 3.6903 | 1.33% |
| 56 | Exp 2_Rate 1.5_pos#14 | 2.4149 | 0.87% |
| 60 | Exp 2_Rate 1.5_pos#15 | 1.9934 | 0.72% |
| 64 | Exp 2_Rate 1.5_pos#16 | 1.5624 | 0.56% |
| 68 | Exp 2_Rate 1.5_pos#17 | 1.2225 | 0.44% |
| 72 | Exp 2_Rate 1.5_pos#18 | 1.0981 | 0.39% |
| 76 | Exp 2_Rate 1.5_pos#19 | 0.8186 | 0.29% |
| 80 | Exp 2_Rate 1.5_pos#20 | 0.6435 | 0.23% |
| 84 | Exp 2_Rate 1.5_pos#21 | 0.4414 | 0.16% |
| 88 | Exp 2_Rate 1.5_pos#22 | 0.3194 | 0.11% |
| 92 | Exp 2_Rate 1.5_pos#23 | 0.2239 | 0.08% |
| 96 | Exp 2_Rate 1.5_pos#24 | 0.1544 | 0.06% |
| 100 | Exp 2_Rate 1.5_pos#25 | 0.0469 | 0.02% |

**Table 7:** IC raw data collected from flow rate experiment 3

| Deployment Time (min) | Exp#_DripRate_Vial ID | Chloride Amount (mg/L) | Normalised Concentration |
|---|---|---|---|
| 4 | Exp 3_Rate 1.0_pos#1 | 217.8419 | 100.00% |
| 8 | Exp 3_Rate 1.0_pos#2 | 121.5723 | 55.81% |
| 12 | Exp 3_Rate 1.0_pos#3 | 74.2913 | 34.10% |
| 16 | Exp 3_Rate 1.0_pos#4 | 50.8067 | 23.32% |
| 20 | Exp 3_Rate 1.0_pos#5 | 36.5692 | 16.79% |
| 24 | Exp 3_Rate 1.0_pos#6 | 29.9339 | 13.74% |
| 28 | Exp 3_Rate 1.0_pos#7 | 28.6837 | 13.17% |
| 32 | Exp 3_Rate 1.0_pos#8 | 20.6825 | 9.49% |
| 36 | Exp 3_Rate 1.0_pos#9 | 15.4467 | 7.09% |
| 40 | Exp 3_Rate 1.0_pos#10 | 10.9707 | 5.04% |
| 44 | Exp 3_Rate 1.0_pos#11 | 7.5503 | 3.47% |
| 48 | Exp 3_Rate 1.0_pos#12 | 5.3168 | 2.44% |
| 52 | Exp 3_Rate 1.0_pos#13 | 3.8627 | 1.77% |
| 56 | Exp 3_Rate 1.0_pos#14 | 2.7168 | 1.25% |
| 60 | Exp 3_Rate 1.0_pos#15 | 1.9562 | 0.90% |
| 64 | Exp 3_Rate 1.0_pos#16 | 1.3672 | 0.63% |
| 68 | Exp 3_Rate 1.0_pos#17 | 1.0351 | 0.48% |
| 72 | Exp 3_Rate 1.0_pos#18 | 0.5861 | 0.27% |
| 76 | Exp 3_Rate 1.0_pos#19 | 0.2573 | 0.12% |
| 80 | Exp 3_Rate 1.0_pos#20 | 0.0416 | 0.02% |

**Table 8:** IC raw data collected from flow rate experiment 4

| Deployment Time (min) | Exp#_DripRate_Vial ID | Chloride Amount (mg/L) | Normalised Concentration |
|---|---|---|---|
| 4 | Exp 4_Rate 1.0_pos#1 | 219.3906 | 100.00% |
| 8 | Exp 4_Rate 1.0_pos#2 | 128.3632 | 58.51% |
| 12 | Exp 4_Rate 1.0_pos#3 | 78.1022 | 35.60% |
| 16 | Exp 4_Rate 1.0_pos#4 | 39.105 | 17.82% |
| 20 | Exp 4_Rate 1.0_pos#5 | 4.2765 | 1.95% |
| 24 | Exp 4_Rate 1.0_pos#6 | 19.978 | 9.11% |
| 28 | Exp 4_Rate 1.0_pos#7 | 15.5119 | 7.07% |
| 32 | Exp 4_Rate 1.0_pos#8 | 12.0247 | 5.48% |
| 36 | Exp 4_Rate 1.0_pos#9 | 9.7941 | 4.46% |
| 40 | Exp 4_Rate 1.0_pos#10 | 7.9971 | 3.65% |
| 44 | Exp 4_Rate 1.0_pos#11 | 8.5317 | 3.89% |
| 48 | Exp 4_Rate 1.0_pos#12 | 5.9663 | 2.72% |
| 52 | Exp 4_Rate 1.0_pos#13 | 4.7816 | 2.18% |
| 56 | Exp 4_Rate 1.0_pos#14 | 4.6809 | 2.13% |
| 60 | Exp 4_Rate 1.0_pos#15 | 3.2858 | 1.50% |
| 64 | Exp 4_Rate 1.0_pos#16 | 2.8127 | 1.28% |
| 68 | Exp 4_Rate 1.0_pos#17 | 2.3605 | 1.08% |
| 72 | Exp 4_Rate 1.0_pos#18 | 1.9023 | 0.87% |
| 76 | Exp 4_Rate 1.0_pos#19 | 1.5463 | 0.70% |
| 80 | Exp 4_Rate 1.0_pos#20 | 1.695 | 0.77% |

**Table 9:** IC raw data collected from flow rate experiment 5

| Deployment Time (min) | Exp#_DripRate_Vial ID | Chloride Amount (mg/L) | Normalised Concentration |
|---|---|---|---|
| 4 | Exp 5_Rate 0.5_pos#1 | 198.5883 | 100.00% |
| 8 | Exp 5_Rate 0.5_pos#2 | 116.625 | 58.73% |
| 12 | Exp 5_Rate 0.5_pos#3 | 89.469 | 45.05% |
| 16 | Exp 5_Rate 0.5_pos#4 | 63.9842 | 32.22% |
| 20 | Exp 5_Rate 0.5_pos#5 | 43.3486 | 21.83% |
| 24 | Exp 5_Rate 0.5_pos#6 | 31.0259 | 15.62% |
| 28 | Exp 5_Rate 0.5_pos#7 | 23.2379 | 11.70% |
| 32 | Exp 5_Rate 0.5_pos#8 | 18.18 | 9.15% |
| 36 | Exp 5_Rate 0.5_pos#9 | 14.2298 | 7.17% |
| 40 | Exp 5_Rate 0.5_pos#10 | 11.4085 | 5.74% |
| 44 | Exp 5_Rate 0.5_pos#11 | 9.1044 | 4.58% |
| 48 | Exp 5_Rate 0.5_pos#12 | 7.3956 | 3.72% |
| 52 | Exp 5_Rate 0.5_pos#13 | 7.2082 | 3.63% |
| 56 | Exp 5_Rate 0.5_pos#14 | 7.6068 | 3.83% |
| 60 | ~~Exp 5_Rate 0.5_pos#15~~ | ~~n.a.~~ | ~~n.a.~~ |
| 64 | Exp 5_Rate 0.5_pos#16 | 4.2867 | 2.16% |
| 68 | Exp 5_Rate 0.5_pos#17 | 3.4215 | 1.72% |
| 72 | Exp 5_Rate 0.5_pos#18 | 2.7387 | 1.38% |
| 76 | Exp 5_Rate 0.5_pos#19 | 2.0971 | 1.06% |
| 80 | Exp 5_Rate 0.5_pos#20 | 1.2217 | 0.62% |
| 84 | Exp 5_Rate 0.5_pos#21 | 0.8156 | 0.41% |
| 88 | Exp 5_Rate 0.5_pos#22 | 0.5007 | 0.25% |
| 92 | Exp 5_Rate 0.5_pos#23 | 1.0095 | 0.51% |
| 96 | Exp 5_Rate 0.5_pos#24 | 0.6394 | 0.32% |
| 100 | Exp 5_Rate 0.5_pos#25 | 0.5459 | 0.27% |
| 104 | Exp 5_Rate 0.5_pos#26 | 0.4717 | 0.24% |
| 108 | Exp 5_Rate 0.5_pos#27 | 0.4088 | 0.21% |
| 112 | Exp 5_Rate 0.5_pos#28 | 0.3689 | 0.19% |
| 116 | Exp 5_Rate 0.5_pos#29 | 0.3421 | 0.17% |
| 120 | Exp 5_Rate 0.5_pos#30 | 0.3496 | 0.18% |

**Table 10:** IC raw data collected from flow rate experiment 6

| Deployment Time (min) | Exp#_DripRate_Vial ID | Chloride Amount (mg/L) | Normalised Concentration |
|---|---|---|---|
| 4 | Exp 6_Rate 0.5_pos#1 | 223.9305 | 100.00% |
| 8 | Exp 6_Rate 0.5_pos#2 | 147.3432 | 65.80% |
| 12 | Exp 6_Rate 0.5_pos#3 | 106.738 | 47.67% |
| 16 | Exp 6_Rate 0.5_pos#4 | 80.5036 | 35.95% |
| 20 | Exp 6_Rate 0.5_pos#5 | 64.9124 | 28.99% |
| 24 | Exp 6_Rate 0.5_pos#6 | 51.7498 | 23.11% |
| 28 | Exp 6_Rate 0.5_pos#7 | 41.5835 | 18.57% |
| 32 | Exp 6_Rate 0.5_pos#8 | 34.4560 | 15.39% |
| 36 | Exp 6_Rate 0.5_pos#9 | 29.4717 | 13.16% |
| 40 | Exp 6_Rate 0.5_pos#10 | 24.9686 | 11.15% |
| 44 | Exp 6_Rate 0.5_pos#11 | 22.2846 | 9.95% |
| 48 | Exp 6_Rate 0.5_pos#12 | 19.4941 | 8.71% |
| 52 | Exp 6_Rate 0.5_pos#13 | 17.0995 | 7.64% |
| 56 | Exp 6_Rate 0.5_pos#14 | 14.8409 | 6.63% |
| 60 | Exp 6_Rate 0.5_pos#15 | 12.9727 | 5.79% |
| 64 | Exp 6_Rate 0.5_pos#16 | 11.0259 | 4.92% |
| 68 | Exp 6_Rate 0.5_pos#17 | 9.4532 | 4.22% |
| 72 | Exp 6_Rate 0.5_pos#18 | 7.7772 | 3.47% |
| 76 | Exp 6_Rate 0.5_pos#19 | 6.8732 | 3.07% |
| 80 | Exp 6_Rate 0.5_pos#20 | 5.9131 | 2.64% |
| 84 | Exp 6_Rate 0.5_pos#21 | 4.7371 | 2.12% |
| 88 | Exp 6_Rate 0.5_pos#22 | 3.9801 | 1.78% |
| 92 | Exp 6_Rate 0.5_pos#23 | 3.2225 | 1.44% |
| 96 | Exp 6_Rate 0.5_pos#24 | 3.1030 | 1.39% |
| 100 | Exp 6_Rate 0.5_pos#25 | 2.6350 | 1.18% |
| 104 | Exp 6_Rate 0.5_pos#26 | 1.8943 | 0.85% |
| 108 | Exp 6_Rate 0.5_pos#27 | 1.8267 | 0.82% |
| 112 | Exp 6_Rate 0.5_pos#28 | 1.2686 | 0.57% |
| 116 | Exp 6_Rate 0.5_pos#29 | 0.8951 | 0.40% |
| 120 | Exp 6_Rate 0.5_pos#30 | 0.6568 | 0.29% |

a

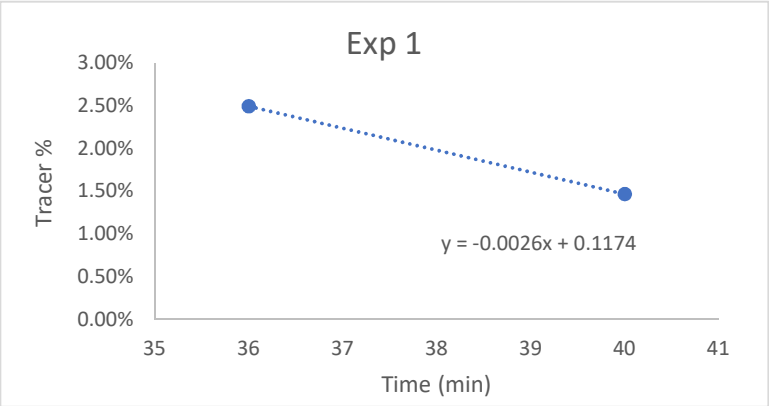


b

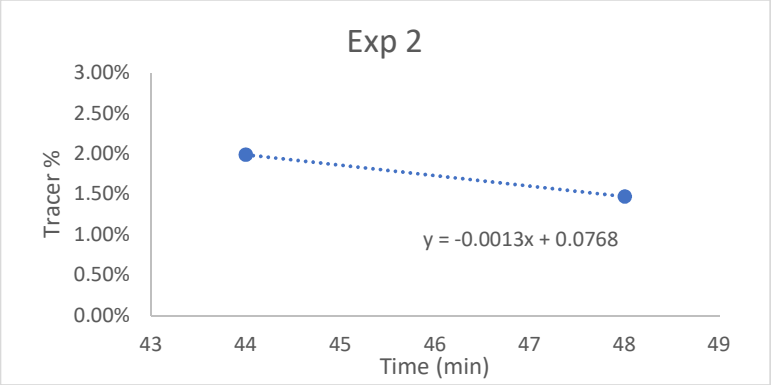


c

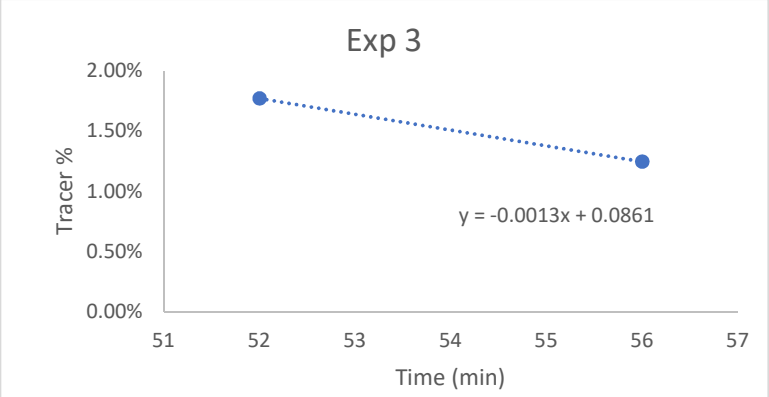


continued

e

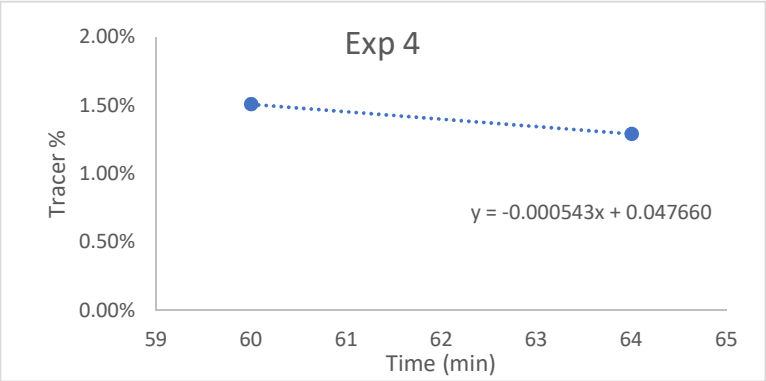


f

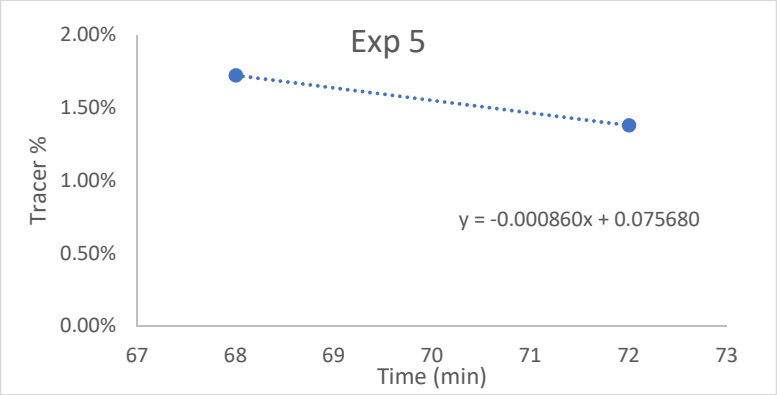


g

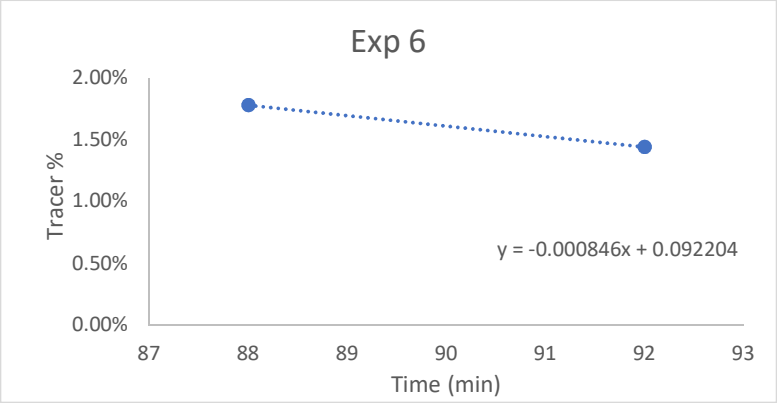


**Figure 18:** Relationship between deployment time and remaining tracer within the resin gel.

**Table 11:** Summary of flow rate experiment

| Exp# | Drip Rate (mL/min) | Time (min) | Tracer (%) | Time at 6 PV (min) | Time at 1 PV (min) | Gel Length (cm) | Flow Rate within Resin Gel (cm/min) |
|---|---|---|---|---|---|---|---|
| 1 | 1.5 | 36 | 2.492% | 39 | 7.19 | 30 | 4.17 |
| | | 40 | 1.465% | | | | |
| 2 | 1.5 | 44 | 1.989% | 47 | | | |
| | | 48 | 1.471% | | | | |
| 3 | 1 | 52 | 1.77% | 54 | 9.44 | 30 | 3.18 |
| | | 56 | 1.25% | | | | |
| 4 | 1 | 60 | 1.51% | 59 | | | |
| | | 64 | 1.29% | | | | |
| 5 | 0.5 | 68 | 1.723% | 70 | 13.4 | 30 | 2.24 |
| | | 72 | 1.379% | | | | |
| 6 | 0.5 | 88 | 1.78% | 91 | | | |
| | | 92 | 1.44% | | | | |

## Appendix II: Analysis of Metal Accumulation Experiment Data

Number annotations for tables 12-15:

1. The volume of one gel slice is calculated as: a Chelex resin gel disc has an area of 3.14 $cm^2$ and a volume of 0.16 mL (Lehto, 2016). Hence, a 1 $cm^2$ gel slice has a volume of 0.051 mL. Influent and effluent samples do not contain gel slices.
2. Concentration of Ni in eluate = concentration of nickel in ICP-MS sample solution × cumulative volume ÷ eluate volume
3. Mass of Ni in eluate= concentration of nickel in ICP-MS sample solution × cumulative volume

**Table 12:** Calculation of accumulated nickel on resin gel in metal accumulation experiment A

| Distance (cm) | Sample ID | Eluate Volume incl. Gel [1] +$HNO_3$ (mL) | H2O (mL) | Cumulative Volume (mL) | Na ICP-MS Raw Data (ng/mL) | Ni ICP-MS Raw Data (ng/mL) | Ni in Eluate [2] (ug/mL) | Mass of Ni [3] (ug) |
|---|---|---|---|---|---|---|---|---|
| 1 | Exp A_pos#1 | 1.051 | 4.0 | 5.051 | 18058.342 | 129.482 | 0.62 | 0.65 |
| 2 | Exp A_pos#2 | 1.051 | 4.0 | 5.051 | 19177.002 | 135.105 | 0.65 | 0.68 |
| 3 | Exp A_pos#3 | 1.051 | 4.0 | 5.051 | 21890.437 | 151.475 | 0.73 | 0.77 |
| 4 | Exp A_pos#4 | 1.051 | 4.0 | 5.051 | 20791.446 | 137.539 | 0.66 | 0.69 |
| 5 | Exp A_pos#5 | 1.051 | 4.0 | 5.051 | 18997.122 | 128.181 | 0.62 | 0.65 |
| 9 | Exp A_pos#9 | 1.051 | 4.0 | 5.051 | 18685.886 | 123.805 | 0.59 | 0.63 |
| 13 | Exp A_pos#13 | 1.051 | 4.0 | 5.051 | 16202.775 | 110.476 | 0.53 | 0.56 |
| 17 | Exp A_pos#17 | 1.051 | 4.0 | 5.051 | 16368.358 | 110.505 | 0.53 | 0.56 |
| 21 | Exp A_pos#21 | 1.051 | 4.0 | 5.051 | 16855.035 | 113.334 | 0.54 | 0.57 |
| 25 | Exp A_pos#25 | 1.051 | 4.0 | 5.051 | 16008.381 | 105.263 | 0.51 | 0.53 |
| 26 | Exp A_pos#26 | 1.051 | 4.0 | 5.051 | 15752.447 | 102.411 | 0.49 | 0.52 |
| 27 | Exp A_pos#27 | 1.051 | 4.0 | 5.051 | 15751.673 | 109.813 | 0.53 | 0.55 |
| 28 | Exp A_pos#28 | 1.051 | 4.0 | 5.051 | 13692.703 | 98.786 | 0.47 | 0.50 |
| - | Exp A_0h influent | 5.1 | - | 5.1 | 683620.1 | 4796.204 | 4.80 | - |
| - | Exp A_0h effluent | 5.1 | - | 5.1 | 633658.1 | 4214.778 | 4.21 | - |
| - | Exp A_5h influent | 5.1 | - | 5.1 | 674400.3 | 4873.175 | 4.87 | - |
| - | Exp A_5h effluent | 5.1 | - | 5.1 | 684518.57 | 4919.441 | 4.92 | - |

**Table 13:** Calculation of accumulated nickel on resin gel in metal accumulation experiment B

| Distance (cm) | Sample ID | Eluate Volume incl. Gel [1] +$HNO_3$ (mL) | H2O (mL) | Cumulative Volume (mL) | Na ICP-MS Raw Data (ng/mL) | Ni ICP-MS Raw Data (ng/mL) | Ni in Eluate [2] (ug/mL) | Mass of Ni [3] (ug) |
|---|---|---|---|---|---|---|---|---|
| 1 | Exp B_pos#1 | 1.051 | 4.0 | 5.051 | 42693.816 | 169.39 | 0.81 | 0.86 |
| 2 | Exp B_ pos#2 | 1.051 | 4.0 | 5.051 | 27532.553 | 106.193 | 0.51 | 0.54 |
| 3 | Exp B_ pos#3 | 1.051 | 4.0 | 5.051 | 18490.568 | 69.461 | 0.33 | 0.35 |
| 4 | Exp B_ pos#4 | 1.051 | 4.0 | 5.051 | 13667.967 | 52.500 | 0.25 | 0.27 |
| 5 | Exp B_ pos#5 | 1.051 | 4.0 | 5.051 | 14564.545 | 54.895 | 0.26 | 0.28 |
| 9 | Exp B_ pos#9 | 1.051 | 4.0 | 5.051 | 14347.217 | 55.148 | 0.27 | 0.28 |
| 13 | Exp B_ pos#13 | 1.051 | 4.0 | 5.051 | 13547.507 | 50.562 | 0.24 | 0.26 |
| 17 | Exp B_ pos#17 | 1.051 | 4.0 | 5.051 | 13682.182 | 50.999 | 0.25 | 0.26 |
| 21 | Exp B_ pos#21 | 1.051 | 4.0 | 5.051 | 12285.387 | 46.534 | 0.22 | 0.24 |
| 25 | Exp B_ pos#25 | 1.051 | 4.0 | 5.051 | 12089.609 | 44.718 | 0.21 | 0.23 |
| 26 | Exp B_ pos#26 | 1.051 | 4.0 | 5.051 | 10975.485 | 41.689 | 0.20 | 0.21 |
| 27 | Exp B_ pos#27 | 1.051 | 4.0 | 5.051 | 11371.453 | 42.671 | 0.21 | 0.22 |
| 28 | Exp B_ pos#28 | 1.051 | 4.0 | 5.051 | 12028.085 | 43.958 | 0.21 | 0.22 |
| - | Exp B_0h influent | 5.1 | - | 5.1 | 670527.99 | 2373.747 | 2.37 | - |
| - | Exp B_0h effluent | 5.1 | - | 5.1 | 614559.35 | 2084.917 | 2.08 | - |
| - | Exp B_5h influent | 5.1 | - | 5.1 | 705050.42 | 2480.948 | 2.48 | - |
| - | Exp B_5h effluent | 5.1 | - | 5.1 | 706737.41 | 2449.297 | 2.45 | - |

**Table 14:** Calculation of accumulated nickel on resin gel in metal accumulation experiment C

| Distance (cm) | Sample ID | Eluate Volume incl. Gel [1] +$HNO_3$ (mL) | H2O (mL) | Cumulative Volume (mL) | Na ICP-MS Raw Data (ng/mL) | Ni ICP-MS Raw Data (ng/mL) | Ni in Eluate [2] (ug/mL) | Mass of Ni [3] (ug) |
|---|---|---|---|---|---|---|---|---|
| 1 | Exp C_pos#1 | 1.051 | 4.0 | 5.051 | 15684.176 | 33.329 | 0.16 | 0.17 |
| 2 | Exp C_pos#2 | 1.051 | 4.0 | 5.051 | 17092.196 | 36.416 | 0.18 | 0.18 |
| 3 | Exp C_pos#3 | 1.051 | 4.0 | 5.051 | 17949.805 | 37.302 | 0.18 | 0.19 |
| 4 | Exp C_pos#4 | 1.051 | 4.0 | 5.051 | 18940.645 | 38.938 | 0.19 | 0.20 |
| 5 | Exp C_pos#5 | 1.051 | 4.0 | 5.051 | 16121.234 | 33.217 | 0.16 | 0.17 |
| 9 | Exp C_pos#9 | 1.051 | 4.0 | 5.051 | 15262.703 | 30.226 | 0.15 | 0.15 |
| 13 | Exp C_pos#13 | 1.051 | 4.0 | 5.051 | 16026.79 | 32.313 | 0.16 | 0.16 |
| 17 | Exp C_pos#17 | 1.051 | 4.0 | 5.051 | 15500.735 | 31.264 | 0.15 | 0.16 |
| 21 | Exp C_pos#21 | 1.051 | 4.0 | 5.051 | 14188.851 | 28.099 | 0.14 | 0.14 |
| 25 | Exp C_pos#25 | 1.051 | 4.0 | 5.051 | 14098.018 | 27.614 | 0.13 | 0.14 |
| 26 | Exp C_pos#26 | 1.051 | 4.0 | 5.051 | 14164.773 | 28.125 | 0.14 | 0.14 |
| 27 | Exp C_pos#27 | 1.051 | 4.0 | 5.051 | 16012.827 | 31.112 | 0.15 | 0.16 |
| 28 | Exp C_pos#28 | 1.051 | 4.0 | 5.051 | 13060.792 | 26.380 | 0.13 | 0.13 |
| - | Exp C_0h influent | 5.1 | - | 5.1 | 717994.8 | 1268.832 | 1.27 | - |
| - | Exp C_0h effluent | 5.1 | - | 5.1 | 672134.8 | 1127.876 | 1.13 | - |
| - | Exp C_5h influent | 5.1 | - | 5.1 | 676787.95 | 1215.136 | 1.22 | - |
| - | Exp C_5h effluent | 5.1 | - | 5.1 | 701273.33 | 1220.973 | 1.22 | - |

**Table 15:** Calculation of accumulated nickel on resin gel in metal accumulation experiment D

| Distance (cm) | Sample ID | Eluate Volume incl. Gel [1] +$HNO_3$ (mL) | H2O (mL) | Cumulative Volume (mL) | Na ICP-MS Raw Data (ng/mL) | Ni ICP-MS Raw Data (ng/mL) | Ni in Eluate [2] (ug/mL) | Mass of Ni [3] (ug) |
|---|---|---|---|---|---|---|---|---|
| 1 | Exp D_pos#1 | 1.051 | 4.0 | 5.051 | 37129.978 | 1156.237 | 5.56 | 5.84 |
| 2 | Exp D_pos#2 | 1.051 | 4.0 | 5.051 | 15163.999 | 764.297 | 3.67 | 3.86 |
| 3 | Exp D_pos#3 | 1.051 | 4.0 | 5.051 | 16638.588 | 637.936 | 3.07 | 3.22 |
| 4 | Exp D_pos#4 | 1.051 | 4.0 | 5.051 | 16528.125 | 470.241 | 2.26 | 2.38 |
| 5 | Exp D_pos#5 | 1.051 | 4.0 | 5.051 | 16194.827 | 397.300 | 1.91 | 2.01 |
| 9 | Exp D_pos#9 | 1.051 | 4.0 | 5.051 | 17303.247 | 331.303 | 1.59 | 1.67 |
| 13 | Exp D_pos#13 | 1.051 | 4.0 | 5.051 | 16349.664 | 316.855 | 1.52 | 1.60 |
| 17 | Exp D_pos#17 | 1.051 | 4.0 | 5.051 | 16637.016 | 498.112 | 2.39 | 2.52 |
| 21 | Exp D_pos#21 | 1.051 | 4.0 | 5.051 | 18819.053 | 440.264 | 2.12 | 2.22 |
| 25 | Exp D_pos#25 | 1.051 | 4.0 | 5.051 | 16751.97 | 762.556 | 3.66 | 3.85 |
| 26 | Exp D_pos#26 | 1.051 | 4.0 | 5.051 | 15361.454 | 528.742 | 2.54 | 2.67 |
| 27 | Exp D_pos#27 | 1.051 | 4.0 | 5.051 | 15724.059 | 411.093 | 1.98 | 2.08 |
| 28 | Exp D_pos#28 | 1.051 | 4.0 | 5.051 | 14432.290 | 238.500 | 1.15 | 1.20 |
| - | Exp D_0h influent | 5.1 | - | 5.1 | 675183.26 | 1201.867 | 1.20 | - |
| - | Exp D_0h effluent | 5.1 | - | 5.1 | 648290.82 | 978.392 | 0.98 | - |
| - | Exp D_5h influent | 5.1 | - | 5.1 | 698432.22 | 1161.312 | 1.16 | - |
| - | Exp D_5h effluent | 5.1 | - | 5.1 | 697940.21 | 981.08 | 0.98 | - |

## Appendix III: Reverse Modelling of Ni-NTA Dissociation

Number annotations for tables 16-18:

1. Flow moving distance (cm): numbers in **bold** represent the positions of gel slices selected for ICP-MS analysis as described in section 3.3.1.

   The rest of the samples are in *italic.* The results are calculated theoretically by averaging the amount of nickel in the previously measured sample and the subsequent one.

   Samples at distance "0" cm and "31" cm stand for influent collected from reservoir and effluent collected from the end of the probe.

2. Time (min): When the drip rate is set at 1 mL/min, the flow rate within the resin gel is 3.18 cm/min (see Table 11). In other words, the "unit" time required for the solution to move through 1 cm resin gel is 0.315 min.

3. Mass of Ni (μg): The mass of nickel accumulated in the resin gel for five hours deployment time are listed in Appendix II.

4. Accumulated [Ni] (μg/mL): The concentration of nickel in the resin gel = mass of Ni ÷ the volume of gel (0.051 mL).

5. Accumulated [Ni] per min (ng/mL): This is calculated by dividing the accumulated [Ni] in one resin gel slice (1 cm) by the solution residence time (953.45 min = 5 h x 60min ÷ (1cm ÷ 0.315 min· $cm^{-1}$)).

6. Labile [Ni] in solution (nM): The amount of Ni-NTA dissociated and bound to the resin gel. Elution factor for Chelex resin is 0.80 and the molecular weight of nickel (58.69 g/mol) is applied.

7. Observed total [Ni] (nM): The average concentration of nickel in two influent/effluent samples collected at the beginning and end of individual experiment.

8. Predicted total [Ni] (nM): The theoretical concentration of nickel in the flow as it moves through the resin. It is calculated by deducting the labile [Ni] bound to the resin from the initial observed total [Ni].

9. Labile fraction of Ni (%): The fraction of the Ni-NTA complexes that contributes to [Ni] in the resin gel.

**Table 16:** Reverse modelling of metal accumulation experiment A

| Distance [1] (cm) | Time (min) | Mass of Ni [3] (µg) | Accumulated [Ni] [4] (µg/mL) | Accumulated [Ni] per Min [5] (ng/mL) | Labile [Ni] in Solution [6] f=0.8 (nM) | Observed Total [Ni] [7] (nM) | Predicted Total [Ni] [8] (nM) | Labile Fraction of [Ni] [9] (%) |
|---|---|---|---|---|---|---|---|---|
| **0** | **0** | **-** | **-** | **-** | **-** | **82.38** | **-** | |
| **1** | **0.31** | **0.65** | **12.84** | **13.5** | **0.287** | | **82.1** | |
| **2** | **0.63** | **0.68** | **13.39** | **14.0** | **0.299** | | **81.8** | |
| **3** | **0.94** | **0.77** | **15.02** | **15.7** | **0.335** | | **81.5** | |
| **4** | **1.26** | **0.69** | **13.63** | **14.3** | **0.305** | | **81.2** | |
| **5** | **1.57** | **0.65** | **12.71** | **13.3** | **0.284** | | **80.9** | **0.35%** |
| *6* | *1.89* | *0.64* | *12.49* | *13.1* | *0.279* | | *80.6* | |
| *7* | *2.20* | *0.64* | *12.49* | *13.1* | *0.279* | | *80.3* | |
| *8* | *2.52* | *0.64* | *12.49* | *13.1* | *0.279* | | *80.0* | |
| **9** | **2.83** | **0.63** | **12.27** | **12.9** | **0.274** | | **79.8** | **0.34%** |
| *10* | *3.15* | *0.59* | *11.61* | *12.2* | *0.259* | | *79.5* | |
| *11* | *3.46* | *0.59* | *11.61* | *12.2* | *0.259* | | *79.2* | |
| *12* | *3.78* | *0.59* | *11.61* | *12.2* | *0.259* | | *79.0* | |
| **13** | **4.09** | **0.56** | **10.95** | **11.5** | **0.245** | | **78.7** | **0.31%** |
| *14* | *4.41* | *0.56* | *10.95* | *11.5* | *0.245* | | *78.5* | |
| *15* | *4.72* | *0.56* | *10.95* | *11.5* | *0.245* | | *78.2* | |
| *16* | *5.03* | *0.56* | *10.95* | *11.5* | *0.245* | | *78.0* | |

| Distance [1] (cm) | Time (min) | Mass of Ni [3] (µg) | Accumulated [Ni] [4] (µg/mL) | Accumulated [Ni] per Min [5] (ng/mL) | Labile [Ni] in Solution [6] f=0.8 (nM) | Observed Total [Ni] [7] (nM) | Predicted Total [Ni] [8] (nM) | Labile Fraction of [Ni] [9] (%) |
|---|---|---|---|---|---|---|---|---|
| **17** | 5.35 | 0.56 | 10.95 | 11.5 | 0.245 | | 77.8 | 0.31% |
| *18* | *5.66* | *0.57* | *11.09* | *11.6* | *0.248* | | *77.5* | |
| *19* | *5.98* | *0.57* | *11.09* | *11.6* | *0.248* | | *77.3* | |
| *20* | *6.29* | *0.57* | *11.09* | *11.6* | *0.248* | | *77.0* | |
| **21** | **6.61** | **0.57** | **11.23** | **11.8** | **0.251** | | **76.8** | **0.33%** |
| *22* | *6.92* | *0.55* | *10.83* | *11.4* | *0.242* | | *76.5* | |
| *23* | *7.24* | *0.55* | *10.83* | *11.4* | *0.242* | | *76.3* | |
| *24* | *7.55* | *0.55* | *10.83* | *11.4* | *0.242* | | *76.0* | |
| **25** | **7.87** | **0.53** | **10.43** | **10.9** | **0.233** | | **75.8** | **0.31%** |
| **26** | **8.18** | **0.52** | **10.15** | **10.6** | **0.227** | | **75.6** | |
| **27** | **8.50** | **0.55** | **10.89** | **11.4** | **0.243** | | **75.3** | |
| **28** | **8.81** | **0.50** | **9.79** | **10.3** | **0.219** | | **75.1** | |
| *29* | *9.12* | *0.50* | *9.79* | *10.3* | *0.219* | | *74.9* | |
| *30* | *9.44* | *0.68* | *13.29* | *13.9* | *0.297* | | *74.6* | |
| ***31*** | **9.75** | **-** | **-** | **-** | **-** | **77.82** | **-** | |

**Table 17:** Reverse modelling of metal accumulation experiment B

| Distance [1] (cm) | Time (min) | Mass of Ni [3] (µg) | Accumulated [Ni] [4] (µg/mL) | Accumulated [Ni] per Min [5] (ng/mL) | Labile [Ni] in Solution [6] f=0.8 (nM) | Observed Total [Ni] [7] (nM) | Predicted Total [Ni] [8] (nM) | Labile Fraction of [Ni] [9] (%) |
|---|---|---|---|---|---|---|---|---|
| **0** | **0** | **-** | **-** | **-** | **-** | **41.36** | **-** | |
| **1** | **0.31** | **0.86** | **16.79** | **17.6** | **0.375** | **-** | **41.0** | |
| **2** | **0.63** | **0.54** | **10.53** | **11.0** | **0.235** | **-** | **40.7** | |
| **3** | **0.94** | **0.35** | **6.89** | **7.2** | **0.154** | **-** | **40.6** | |
| **4** | **1.26** | **0.27** | **5.20** | **5.5** | **0.116** | **-** | **40.5** | |
| **5** | **1.57** | **0.28** | **5.44** | **5.7** | **0.122** | **-** | **40.4** | **0.30%** |
| *6* | *1.89* | *0.28* | *5.45* | *5.7* | *0.122* | - | *40.2* | |
| *7* | *2.20* | *0.28* | *5.45* | *5.7* | *0.122* | - | *40.1* | |
| *8* | *2.52* | *0.28* | *5.45* | *5.7* | *0.122* | - | *40.0* | |
| **9** | **2.83** | **0.28** | **5.47** | **5.7** | **0.122** | **-** | **39.9** | **0.31%** |
| *10* | *3.15* | *0.27* | *5.24* | *5.5* | *0.117* | - | *39.8* | |
| *11* | *3.46* | *0.27* | *5.24* | *5.5* | *0.117* | - | *39.6* | |
| *12* | *3.78* | *0.27* | *5.24* | *5.5* | *0.117* | - | *39.5* | |
| **13** | **4.09** | **0.26** | **5.01** | **5.3** | **0.112** | **-** | **39.4** | **0.28%** |
| *14* | *4.41* | *0.26* | *5.03* | *5.3* | *0.112* | - | *39.3* | |
| *15* | *4.72* | *0.26* | *5.03* | *5.3* | *0.112* | - | *39.2* | |
| *16* | *5.03* | *0.26* | *5.03* | *5.3* | *0.112* | - | *39.1* | |
| **17** | **5.35** | **0.26** | **5.06** | **5.3** | **0.113** | **-** | **39.0** | **0.29%** |
| *18* | *5.66* | *0.25* | *4.83* | *5.1* | *0.108* | - | *38.8* | |

| Distance [1] (cm) | Time (min) | Mass of Ni [3] (µg) | Accumulated [Ni] [4] (µg/mL) | Accumulated [Ni] per Min [5] (ng/mL) | Labile [Ni] in Solution [6] f=0.8 (nM) | Observed Total [Ni] [7] (nM) | Predicted Total [Ni] [8] (nM) | Labile Fraction of [Ni] [9] (%) |
|---|---|---|---|---|---|---|---|---|
| *19* | *5.98* | *0.25* | *4.83* | *5.1* | *0.108* | *-* | *38.7* | |
| *20* | *6.29* | *0.25* | *4.83* | *5.1* | *0.108* | *-* | *38.6* | |
| **21** | **6.61** | **0.24** | **4.61** | **4.8** | **0.103** | **-** | **38.5** | **0.27%** |
| *22* | *6.92* | *0.23* | *4.52* | *4.7* | *0.101* | *-* | *38.4* | |
| *23* | *7.24* | *0.23* | *4.52* | *4.7* | *0.101* | *-* | *38.3* | |
| *24* | *7.55* | *0.23* | *4.52* | *4.7* | *0.101* | *-* | *38.2* | |
| **25** | **7.87** | **0.23** | **4.43** | **4.6** | **0.099** | **-** | **38.1** | **0.26%** |
| **26** | **8.18** | **0.21** | **4.13** | **4.3** | **0.092** | **-** | **38.0** | |
| **27** | **8.50** | **0.22** | **4.23** | **4.4** | **0.094** | **-** | **37.9** | |
| **28** | **8.81** | **0.22** | **4.36** | **4.6** | **0.097** | **-** | **37.8** | |
| *29* | *9.12* | *0.22* | *4.36* | *4.6* | *0.222* | *-* | *37.6* | |
| *30* | *9.44* | *0.22* | *4.36* | *4.6* | *0.222* | *-* | *37.4* | |
| **31** | **9.75** | **-** | **-** | **-** | **-** | **38.63** | **-** | |

**Table 18:** Reverse modelling of metal accumulation experiment C

| Distance [1] (cm) | Time (min) | Mass of Ni [3] (µg) | Accumulated [Ni] [4] (µg/mL) | Accumulated [Ni] per Min [5] (ng/mL) | Labile [Ni] in Solution [6] f=0.8 (nM) | Observed Total [Ni] [7] (nM) | Predicted Total [Ni] [8] (nM) | Labile Fraction of [Ni] [9] (%) |
|---|---|---|---|---|---|---|---|---|
| **0** | **0** | **-** | **-** | **-** | **-** | **21.16** | **-** | |
| **1** | **0.31** | **0.17** | **3.30** | **3.5** | **0.074** | | **21.1** | |
| **2** | **0.63** | **0.18** | **3.61** | **3.8** | **0.081** | | **21.0** | |
| **3** | **0.94** | **0.19** | **3.70** | **3.9** | **0.083** | | **20.9** | |
| **4** | **1.26** | **0.20** | **3.86** | **4.0** | **0.086** | | **20.8** | |
| **5** | **1.57** | **0.17** | **3.29** | **3.5** | **0.074** | | **20.8** | **0.35%** |
| *6* | *1.89* | *0.16* | *3.14* | *3.3* | *0.070* | | *20.7* | |
| *7* | *2.20* | *0.16* | *3.14* | *3.3* | *0.070* | | *20.6* | |
| *8* | *2.52* | *0.16* | *3.14* | *3.3* | *0.070* | | *20.6* | |
| **9** | **2.83** | **0.15** | **3.00** | **3.1** | **0.067** | | **20.5** | **0.33%** |
| *10* | *3.15* | *0.16* | *3.10* | *3.3* | *0.069* | | *20.4* | |
| *11* | *3.46* | *0.16* | *3.10* | *3.3* | *0.069* | | *20.3* | |
| *12* | *3.78* | *0.16* | *3.10* | *3.3* | *0.069* | | *20.3* | |
| **13** | **4.09** | **0.16** | **3.20** | **3.4** | **0.072** | | **20.2** | **0.35%** |
| *14* | *4.41* | *0.16* | *3.15* | *3.3* | *0.070* | | *20.1* | |
| *15* | *4.72* | *0.16* | *3.15* | *3.3* | *0.070* | | *20.1* | |
| *16* | *5.03* | *0.16* | *3.15* | *3.3* | *0.070* | | *20.0* | |
| **17** | **5.35** | **0.16** | **3.10** | **3.3** | **0.069** | | **19.9** | **0.35%** |
| *18* | *5.66* | *0.15* | *2.94* | *3.1* | *0.066* | | *19.9* | |

| Distance [1] (cm) | Time (min) | Mass of Ni [3] (µg) | Accumulated [Ni] [4] (µg/mL) | Accumulated [Ni] per Min [5] (ng/mL) | Labile [Ni] in Solution [6] f=0.8 (nM) | Observed Total [Ni] [7] (nM) | Predicted Total [Ni] [8] (nM) | Labile Fraction of [Ni] [9] (%) |
|---|---|---|---|---|---|---|---|---|
| *19* | *5.98* | *0.15* | *2.94* | *3.1* | *0.066* | | *19.8* | |
| *20* | *6.29* | *0.15* | *2.94* | *3.1* | *0.066* | | *19.7* | |
| **21** | **6.61** | **0.14** | **2.79** | **2.9** | **0.062** | | **19.7** | **0.32%** |
| *22* | *6.92* | *0.14* | *2.76* | *2.9* | *0.062* | | *19.6* | |
| *23* | *7.24* | *0.14* | *2.76* | *2.9* | *0.062* | | *19.5* | |
| *24* | *7.55* | *0.14* | *2.76* | *2.9* | *0.062* | | *19.5* | |
| **25** | **7.87** | **0.14** | **2.74** | **2.9** | **0.061** | | **19.4** | **0.31%** |
| **26** | **8.18** | **0.14** | **2.79** | **2.9** | **0.062** | | **19.4** | |
| **27** | **8.50** | **0.16** | **3.08** | **3.2** | **0.069** | | **19.3** | |
| **28** | **8.81** | **0.13** | **2.61** | **2.7** | **0.058** | | **19.2** | |
| *29* | *9.12* | *0.13* | *2.55* | *2.7* | *0.059* | | *19.2* | |
| *30* | *9.44* | *0.13* | *2.55* | *2.7* | *0.059* | | *19.1* | |
| **31** | **9.75** | **-** | **-** | **-** | **-** | **20.01** | **-** | |

a

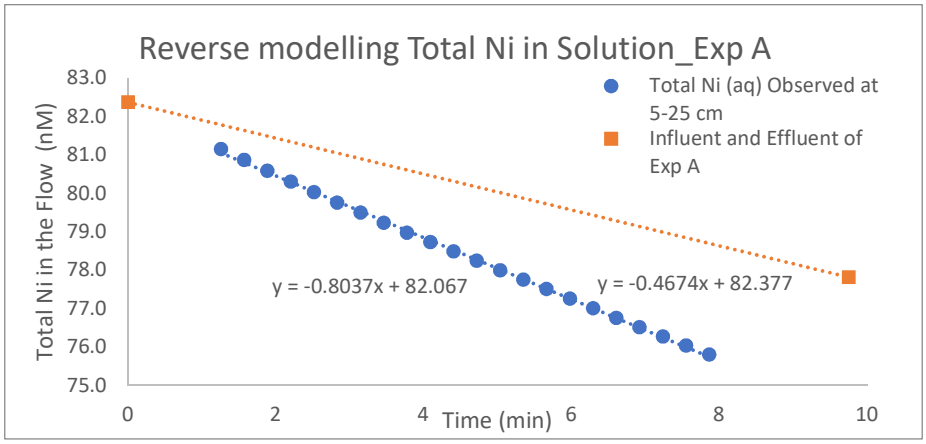


b

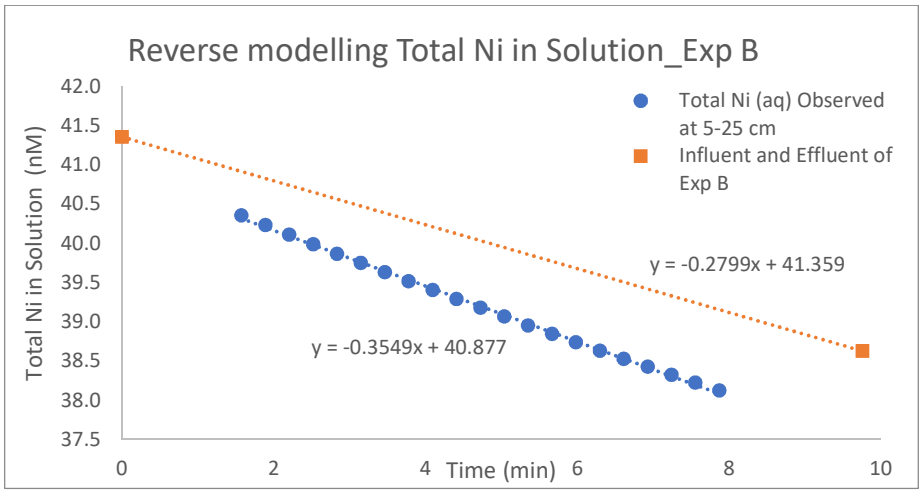


c

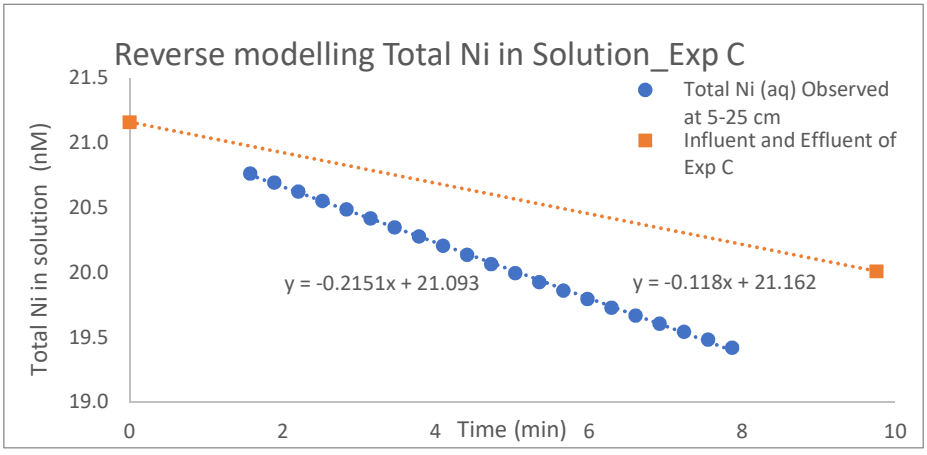


**Figure 19:** Comparison between the observed concentration of total nickel in solution and the theoretical predicted values.

## Appendix IV: Forward Modelling of Ni-NTA Dissociation

Numbered annotations for tables 19-21:

1. Total [Ni] (nM): The concentration of total nickel in the flow before contact with the resin gel. The initial value is the measured concentration of total nickel in the influent sample.

2. Labile [Ni] (nM): $C_i$, the fraction of labile nickel in solution dissociated from Ni-NTA. The averaged value of 0.32 % from Appendix III is used in the forward modelling.

3. Dissociated [Ni] (nM): As discussed in section 3.1.2, the ML complex dissociation reaction obeys first order kinetics. Therefore, the relationship between the concentration of dissociated nickel in solution ($C_t$) and the initial concentration of labile nickel ($C_i$) can be expressed by *Eq 9*:

$$C_t = C_i \times e^{-kt} \qquad \textbf{\textit{Eq 9}}$$

   Where $k$ is the dissociation rate of Ni-NTA, 2.0 x 10-4 $s^{-1}$ (Shafaei Arvajeh et al., 2013). Time ($t$) stands for the flow contact time with 1 cm of resin gel equivalent to 0.315 min (18.8 s).

4. Mass of Ni (ng): The amount of nickel accumulated in one resin gel slice.

5. Predicted [Ni] in Eluate (µg/mL): The mass of nickel in the gel is divided by the volume of the eluate (1.051 mL).

6. Observed [Ni] in Eluate (µg/mL): The ICP-MS measured concentration of nickel in the gel samples over the range 5 to 25 cm.

7. Relative error (%): The difference between the observed values and predicted values is divided by the observed values.

**Table 19:** Forward modelling of metal accumulation experiment A

| Distance (cm) | Total [Ni] [1] (nM) | Labile [Ni] [2] (nM) | Dissociated [Ni] [3] (nM) | Mass of Ni [4] (ng) | Predicted [Ni] in Eluate [5] (μ) | Observed [Ni] in Eluate [6] (μg/mL) | Relative Error [7] (%) |
|---|---|---|---|---|---|---|---|
| 1 | 82.38 | 0.2636 | 0.2626 | 748.8 | 0.5700 | | |
| 2 | 82.11 | 0.2628 | 0.2618 | 746.4 | 0.5682 | | |
| 3 | 81.85 | 0.2619 | 0.2609 | 744.0 | 0.5663 | | |
| 4 | 81.59 | 0.2611 | 0.2601 | 741.7 | 0.5645 | | |
| 5 | 81.33 | 0.2603 | 0.2593 | 739.3 | 0.5627 | 0.6160 | 8.7% |
| 6 | 81.07 | 0.2594 | 0.2585 | 736.9 | 0.5609 | | |
| 7 | 80.81 | 0.2586 | 0.2576 | 734.6 | 0.5592 | | |
| 8 | 80.56 | 0.2578 | 0.2568 | 732.2 | 0.5574 | | |
| 9 | 80.30 | 0.2570 | 0.2560 | 729.9 | 0.5556 | 0.5950 | 6.6% |
| 10 | 80.04 | 0.2561 | 0.2552 | 727.6 | 0.5538 | | |
| 11 | 79.79 | 0.2553 | 0.2544 | 725.3 | 0.5521 | | |
| 12 | 79.53 | 0.2545 | 0.2535 | 723.0 | 0.5503 | | |
| 13 | 79.28 | 0.2537 | 0.2527 | 720.7 | 0.5485 | 0.5309 | 3.3% |
| 14 | 79.03 | 0.2529 | 0.2519 | 718.4 | 0.5468 | | |
| 15 | 78.78 | 0.2521 | 0.2511 | 716.1 | 0.5451 | | |
| 16 | 78.52 | 0.2513 | 0.2503 | 713.8 | 0.5433 | | |
| 17 | 78.27 | 0.2505 | 0.2495 | 711.5 | 0.5416 | 0.5311 | 2.0% |
| 18 | 78.02 | 0.2497 | 0.2487 | 709.2 | 0.5399 | | |
| 19 | 77.78 | 0.2489 | 0.2479 | 707.0 | 0.5381 | | |
| 20 | 77.53 | 0.2481 | 0.2472 | 704.7 | 0.5364 | | |
| 21 | 77.28 | 0.2473 | 0.2464 | 702.5 | 0.5347 | 0.5447 | 1.8% |
| 22 | 77.03 | 0.2465 | 0.2456 | 700.2 | 0.5330 | | |
| 23 | 76.79 | 0.2457 | 0.2448 | 698.0 | 0.5313 | | |
| 24 | 76.54 | 0.2449 | 0.2440 | 695.8 | 0.5296 | | |
| 25 | 76.30 | 0.2442 | 0.2432 | 693.6 | 0.5279 | 0.5059 | 4.4% |
| 26 | 76.06 | 0.2434 | 0.2425 | 691.4 | 0.5262 | | |
| 27 | 75.81 | 0.2426 | 0.2417 | 689.1 | 0.5246 | | |
| 28 | 75.57 | 0.2418 | 0.2409 | 686.9 | 0.5229 | | |
| 29 | 75.33 | 0.2411 | 0.2402 | 684.8 | 0.5212 | | |
| 30 | 75.09 | 0.2403 | 0.2394 | 682.6 | 0.5196 | | |

**Table 20:** Forward modelling of metal accumulation experiment B

| Distance (cm) | Total [Ni] [1] (nM) | Labile [Ni] [2] (nM) | Dissociated [Ni] [3] (nM) | Mass of Ni [4] (ng) | Predicted [Ni] in Eluate [5] (μ) | Observed [Ni] in Eluate [6] (μg/mL) | Relative Error [7] (%) |
|---|---|---|---|---|---|---|---|
| 1 | 41.36 | 0.1323 | 0.1318 | 375.9 | 0.2862 | | |
| 2 | 41.23 | 0.1319 | 0.1314 | 374.8 | 0.2853 | | |
| 3 | 41.10 | 0.1315 | 0.1310 | 373.6 | 0.2843 | | |
| 4 | 40.96 | 0.1311 | 0.1306 | 372.4 | 0.2834 | | |
| 5 | 40.83 | 0.1307 | 0.1302 | 371.2 | 0.2825 | 0.2773 | 1.9% |
| 6 | 40.70 | 0.1303 | 0.1298 | 370.0 | 0.2816 | | |
| 7 | 40.57 | 0.1298 | 0.1293 | 368.8 | 0.2807 | | |
| 8 | 40.44 | 0.1294 | 0.1289 | 367.6 | 0.2798 | | |
| 9 | 40.32 | 0.1290 | 0.1285 | 366.5 | 0.2789 | 0.2650 | 5.2% |
| 10 | 40.19 | 0.1286 | 0.1281 | 365.3 | 0.2781 | | |
| 11 | 40.06 | 0.1282 | 0.1277 | 364.1 | 0.2772 | | |
| 12 | 39.93 | 0.1278 | 0.1273 | 363.0 | 0.2763 | | |
| 13 | 39.80 | 0.1274 | 0.1269 | 361.8 | 0.2754 | 0.2430 | 13.3% |
| 14 | 39.68 | 0.1270 | 0.1265 | 360.7 | 0.2745 | | |
| 15 | 39.55 | 0.1266 | 0.1261 | 359.5 | 0.2737 | | |
| 16 | 39.42 | 0.1262 | 0.1257 | 358.4 | 0.2728 | | |
| 17 | 39.30 | 0.1258 | 0.1253 | 357.2 | 0.2719 | 0.2451 | 10.9% |
| 18 | 39.17 | 0.1254 | 0.1249 | 356.1 | 0.2710 | | |
| 19 | 39.05 | 0.1250 | 0.1245 | 355.0 | 0.2702 | | |
| 20 | 38.92 | 0.1246 | 0.1241 | 353.8 | 0.2693 | | |
| 21 | 38.80 | 0.1242 | 0.1237 | 352.7 | 0.2685 | 0.2236 | 20.0% |
| 22 | 38.68 | 0.1238 | 0.1233 | 351.6 | 0.2676 | | |
| 23 | 38.55 | 0.1234 | 0.1229 | 350.4 | 0.2668 | | |
| 24 | 38.43 | 0.1230 | 0.1225 | 349.3 | 0.2659 | | |
| 25 | 38.31 | 0.1226 | 0.1221 | 348.2 | 0.2651 | 0.2149 | 23.3% |
| 26 | 38.19 | 0.1222 | 0.1217 | 347.1 | 0.2642 | | |
| 27 | 38.06 | 0.1218 | 0.1213 | 346.0 | 0.2634 | | |
| 28 | 37.94 | 0.1214 | 0.1210 | 344.9 | 0.2625 | | |
| 29 | 37.82 | 0.1210 | 0.1206 | 343.8 | 0.2617 | | |
| 30 | 37.70 | 0.1206 | 0.1202 | 342.7 | 0.2609 | | |

**Table 21:** Forward modelling of metal accumulation experiment C

| Distance (cm) | Total [Ni] [1] (nM) | Labile [Ni] [2] (nM) | Dissociated [Ni] [3] (nM) | Mass of Ni [4] (ng) | Predicted [Ni] in Eluate [5] (µ) | Observed [Ni] in Eluate [6] (µg/mL) | Relative Error [7] (%) |
|---|---|---|---|---|---|---|---|
| 1 | 21.16 | 0.0677 | 0.0675 | 192.4 | 0.1464 | | |
| 2 | 21.09 | 0.0675 | 0.0672 | 191.7 | 0.1460 | | |
| 3 | 21.03 | 0.0673 | 0.0670 | 191.1 | 0.1455 | | |
| 4 | 20.96 | 0.0671 | 0.0668 | 190.5 | 0.1450 | | |
| 5 | 20.89 | 0.0669 | 0.0666 | 189.9 | 0.1446 | 0.1596 | 9.4% |
| 6 | 20.83 | 0.0666 | 0.0664 | 189.3 | 0.1441 | | |
| 7 | 20.76 | 0.0664 | 0.0662 | 188.7 | 0.1436 | | |
| 8 | 20.69 | 0.0662 | 0.0660 | 188.1 | 0.1432 | | |
| 9 | 20.63 | 0.0660 | 0.0658 | 187.5 | 0.1427 | 0.1453 | 1.7% |
| 10 | 20.56 | 0.0658 | 0.0656 | 186.9 | 0.1423 | | |
| 11 | 20.50 | 0.0656 | 0.0653 | 186.3 | 0.1418 | | |
| 12 | 20.43 | 0.0654 | 0.0651 | 185.7 | 0.1414 | | |
| 13 | 20.37 | 0.0652 | 0.0649 | 185.1 | 0.1409 | 0.1553 | 9.3% |
| 14 | 20.30 | 0.0650 | 0.0647 | 184.5 | 0.1405 | | |
| 15 | 20.24 | 0.0648 | 0.0645 | 183.9 | 0.1400 | | |
| 16 | 20.17 | 0.0646 | 0.0643 | 183.4 | 0.1396 | | |
| 17 | 20.11 | 0.0643 | 0.0641 | 182.8 | 0.1391 | 0.1503 | 7.4% |
| 18 | 20.04 | 0.0641 | 0.0639 | 182.2 | 0.1387 | | |
| 19 | 19.98 | 0.0639 | 0.0637 | 181.6 | 0.1382 | | |
| 20 | 19.92 | 0.0637 | 0.0635 | 181.0 | 0.1378 | | |
| 21 | 19.85 | 0.0635 | 0.0633 | 180.5 | 0.1374 | 0.1350 | 1.7% |
| 22 | 19.79 | 0.0633 | 0.0631 | 179.9 | 0.1369 | | |
| 23 | 19.73 | 0.0631 | 0.0629 | 179.3 | 0.1365 | | |
| 24 | 19.66 | 0.0629 | 0.0627 | 178.7 | 0.1361 | | |
| 25 | 19.60 | 0.0627 | 0.0625 | 178.2 | 0.1356 | 0.1327 | 2.2% |
| 26 | 19.54 | 0.0625 | 0.0623 | 177.6 | 0.1352 | | |
| 27 | 19.48 | 0.0623 | 0.0621 | 177.0 | 0.1348 | | |
| 28 | 19.41 | 0.0621 | 0.0619 | 176.5 | 0.1343 | | |
| 29 | 19.35 | 0.0619 | 0.0617 | 175.9 | 0.1339 | | |
| 30 | 19.29 | 0.0617 | 0.0615 | 175.3 | 0.1335 | | |

a

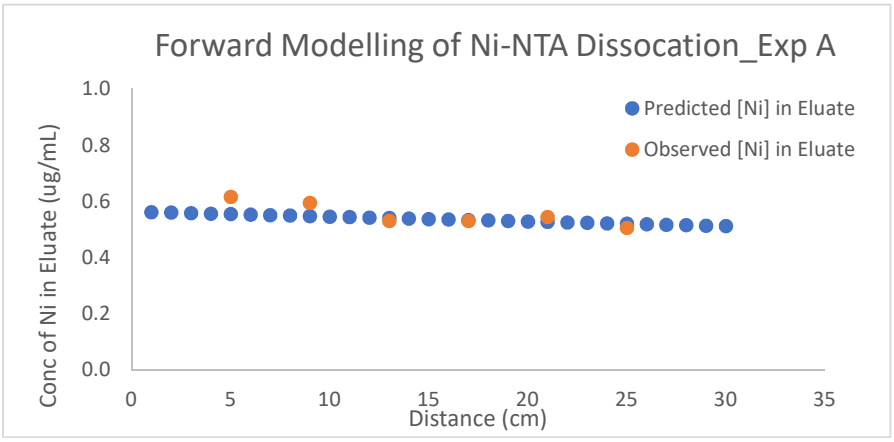


b

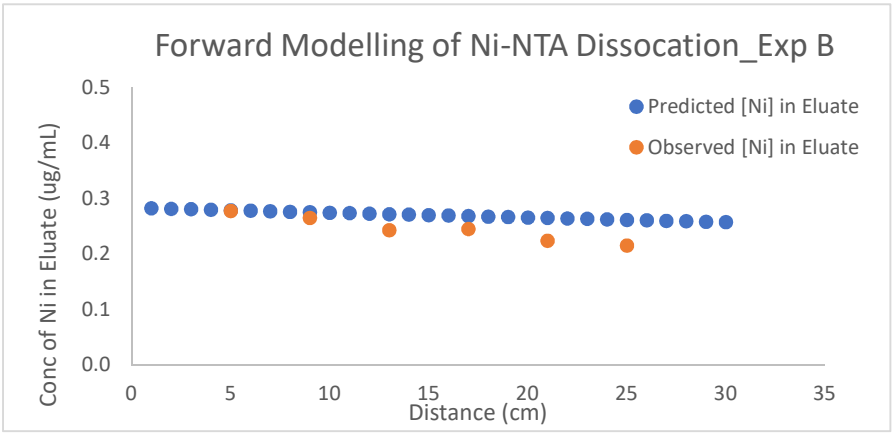


c

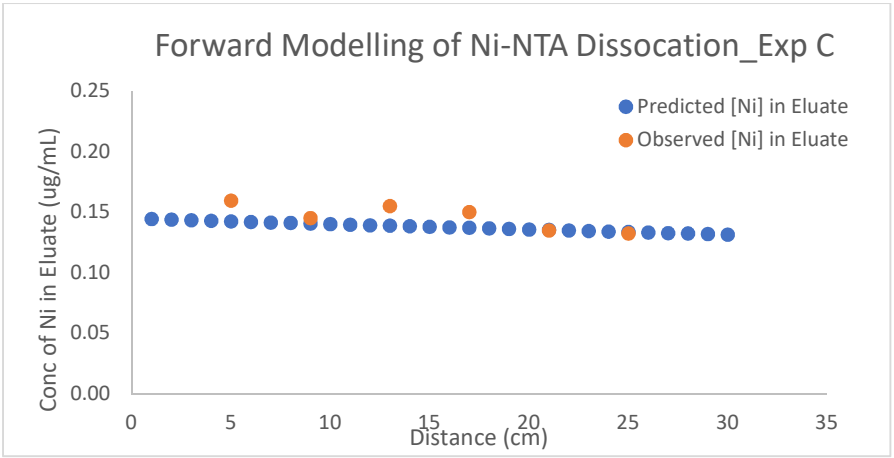


**Figure 20:** The measured concentration of nickel bound to the Chelex resin and the calculated values were plotted against the distance.

# Appendix V: Analysis of Field Experiment Data

**Table 22:** ICP-MS raw data collected from field experiment

| QL [a] | 10 | 70 | 0.2 | 0.3 | 1 | 2 | 0.2 |
|---|---|---|---|---|---|---|---|
| Sample # | $^{23}$Na | $^{40}$Ca | $^{51}$V | $^{52}$Cr | $^{65}$Cu | $^{68}$Zn | $^{89}$Y |
| Gel_1cm | 56.713 | 7745.6 | <0.000 | 0.050 | 0.278 | 4.858 | 0.020 |
| Gel_2cm | 59.213 | 10452.0 | 0.000 | 0.071 | 0.313 | 5.903 | 0.066 |
| Gel_3cm | 45.967 | 11530.0 | 0.003 | 0.092 | 0.304 | 5.163 | 0.156 |
| Gel_4cm | 44.782 | 12829.7 | 0.004 | 0.122 | 0.308 | 5.218 | 0.281 |
| Gel_5cm | 58.965 | 13715.4 | 0.002 | 0.093 | 0.344 | 5.645 | 0.136 |
| Gel_6cm | 45.808 | 12565.7 | <0.000 | 0.066 | 0.289 | 4.551 | 0.046 |
| Gel_7cm | 42.568 | 10366.2 | <0.000 | 0.139 | 0.326 | 4.663 | 0.021 |
| Gel_8cm | 65.640 | 10737.7 | 0.010 | 0.318 | 0.305 | 4.791 | 0.017 |
| Gel_9cm | 46.234 | 11291.7 | 0.013 | 0.421 | 0.302 | 4.322 | 0.028 |
| Gel_10cm | 42.803 | 9805.9 | <0.000 | 0.060 | 0.299 | 4.607 | 0.010 |
| Gel_11cm | 41.518 | 11530.1 | 0.002 | 0.073 | 0.260 | 4.718 | 0.014 |
| Gel_12cm | 44.382 | 13276.0 | 0.000 | 0.066 | 0.252 | 4.518 | 0.008 |
| Drip Water | 3400.65 | 56637.1 | 0.216 | 0.341 | 0.294 | 0.951 | 0.008 |

a. QL: Quantitation Limit, ng/mL.

b. The concentrations of metals are reported in ng/mL.

**Table 23:** Calculation of mass of accumulated metals on resin gel

| Distance (cm) | Vol. of Eluate (mL) | Cumulative Vol. (mL) | Elution Factor f=0.8 | Mass [b] _Cu (ng) | Mass _Zn (ng) | Mass _Cr (ng) | Mass _ Y (ng) |
|---|---|---|---|---|---|---|---|
| 1 | 1.051 | 5.051 | 0.8 | 1.76 | 30.67 | 0.32 | 0.13 |
| 2 | 1.051 | 5.051 | 0.8 | 1.98 | 37.27 | 0.45 | 0.42 |
| 3 | 1.051 | 5.051 | 0.8 | 1.92 | 32.60 | 0.58 | 0.98 |
| 4 | 1.051 | 5.051 | 0.8 | 1.94 | 32.95 | 0.77 | 1.77 |
| 5 | 1.051 | 5.051 | 0.8 | 2.17 | 35.64 | 0.59 | 0.86 |
| 6 | 1.051 | 5.051 | 0.8 | 1.82 | 28.73 | 0.42 | 0.29 |
| 7 | 1.051 | 5.051 | 0.8 | 2.06 | 29.44 | 0.88 | 0.13 |
| 8 | 1.051 | 5.051 | 0.8 | 1.93 | 30.25 | 2.01 | 0.11 |
| 9 | 1.051 | 5.051 | 0.8 | 1.91 | 27.29 | 2.66 | 0.18 |
| 10 | 1.051 | 5.051 | 0.8 | 1.89 | 29.09 | 0.38 | 0.06 |
| 11 | 1.051 | 5.051 | 0.8 | 1.64 | 29.79 | 0.46 | 0.09 |
| 12 | 1.051 | 5.051 | 0.8 | 1.59 | 28.53 | 0.42 | 0.05 |
| Drip water [a] | 5.1 | 5.1 | n/a | 628 | 2031 | 728 | 17 |
| Average Labile Fraction of Metal % | | | | 0.30% | 1.53% | 0.11% | 2.47% |

a. The total amount of metal in dripwater is calculated from the concentration of the metal in dripwater sample and the total volume of dripwater measured (2.18 L).

b. The mass of metal accumulated in the gel = the ICP-MS concentration of the metal × cumulative vol ÷ elution factor (0.8)